

PHOTOSYNTHETIC ADAPTATIONS OF POLAR PHYTOPLANKTON
TO EXTREME LOW LIGHT

BY
NATASHA MADELEINE RYAN

A thesis submitted to the
Department of Biology
Mount Allison University
in partial fulfillment of the requirements for the
Bachelor of Science degree with Honours in Biology
April 19, 2024

Table of Contents

List of Figures	II
List of Tables	IV
Acknowledgements	V
Abstract	VI
Introduction	1
Polar Phytoplankton.....	1
<i>Arctic Blooms</i>	2
<i>Cold Adaptations</i>	3
Energetic Principles of Photosynthesis.....	5
<i>Recombination</i>	6
<i>S-State Cycling</i>	7
Study Aims.....	9
Materials & Methods	10
Study Strains	10
<i>Culturing Protocols</i>	10
Single Turnover Variable Chlorophyll Fluorescence	11
<i>Measurement Conditions</i>	14
Analytical Methods.....	15
<i>Wavelet Transformations</i>	15
<i>Generalized Additive Modelling</i>	17
Results	19
Single Turnover Variable Chlorophyll Fluorescence	19
Wavelet Analysis	19
Generalized Additive Modelling by Deviation from Growth Temperature	21
Generalized Additive Modelling By Measurement Temperature.....	25
Discussion	30
Modelling and Operational Limitations.....	30
Consistent Responses to Measurement Conditions	31
Comparisons Among Strains	32
Ecological Implications & Future Directions	34
References	35
Appendix	41

List of Figures

- Figure 1:** Electron flow through the photosystem II protein complex within the thylakoid membrane of chloroplasts. 5
- Figure 2:** Photodamaging and photoprotective recombination pathways in photosystem II. 7
- Figure 3:** Pathway of S-State cycling and the electron transfer in PSII. Successive PSII charge separations extract successive electrons from the Mn cluster, inducing four increasingly oxidized states. After accumulating four oxidizing equivalents, 2 H₂O molecules are oxidized to 1 O₂ and four protons released to the lumenal side of the thylakoid. 8
- Figure 4:** Sample chlorophyll fluorescence induction curve 12
- Figure 5:** Repeated single-turnover excitation of variable chlorophyll fluorescence for monitoring the S-State cycling in PSII during photosynthesis. Sequential flashes drive S-State transitions from S₀ to S₁, S₁ to S₂, S₂ to S₃, and S₃ to the transient S₄ state, which rapidly decays to S₀. 13
- Figure 6:** Representative wavelet transformation of *Chlamydomonas priscuii* fluorescence over 32 consecutive flashes, measured at 4°C and 1-second flash spacing, equivalent to a photon delivery rate to PSII achieved under an equivalent light level of 0.708 μmol photons m⁻² s⁻¹. 16
- Figure 7:** Sample plot illustrating the wavelet reconstructions at α = 0.05 of *Chlamydomonas priscuii* fluorescence over 32 consecutive single turnover flashes across a range of measurement temperatures and flash spacings, with their equivalent light levels. 17
- Figure 8:** Oscillations in the maximum quantum yield of the photochemistry in *Chlamydomonas priscuii* cultures over a series of 32 flashes, as measured through the secondary chlorophyll fluorescence parameter F_v/F_M. Representative conditions include cultures measured at 4 or 12 °C, with flash spacings of 1, 4, or 16 seconds, equivalent to light levels of 0.045 – 0.708 μmol photons m⁻²s⁻¹. 19
- Figure 9:** Sample plot of wavelet power by period of oscillations in the maximum quantum yield of photochemistry in A. Polar *Chlamydomonas priscuii* and B. Temperate *Chlamydomonas reinhardtii* cultures across a range of measurement temperatures and flash spacings, with the equivalent light levels. 20
- Figure 10:** Statistical significance of 4-step oscillations in the maximum quantum yield of PSII photochemistry across polar and temperate phytoplankton taxa, as measured through variable chlorophyll fluorescence. 21
- Figure 11:** GAM model predictions of the consecutive flashes before the damping of S-State-induced chlorophyll fluorescence oscillations as predicted by the deviation from growth temperature (°C) during measurements and the equivalent light level (μmol photons m⁻²s⁻¹, with equivalent flash spacings in seconds) experienced by polar and temperate diatoms. White dashed lines represent the growth temperatures. 23

Figure 12: GAM model predictions of the consecutive flashes before the damping of S-State-induced chlorophyll fluorescence oscillations as predicted by the deviation from growth temperature (°C) during measurements and the equivalent light level ($\mu\text{mol photons m}^{-2}\text{s}^{-1}$, with equivalent flash spacings in seconds) experienced by polar and temperate green algae. Dashed lines represent the growth temperatures. 24

Figure 13: Statistical significance of 4-step oscillations in the maximum quantum yield of PSII photochemistry across measurement conditions in the polar diatom *F. cylindrus*, as measured through variable chlorophyll fluorescence..... 26

Figure 14: GAM model predictions of the consecutive flashes before the damping of S-State-induced chlorophyll fluorescence oscillations as predicted by the measurement temperature (°C) and equivalent light level ($\mu\text{mol photons m}^{-2}\text{s}^{-1}$; with equivalent flash spacings in seconds) experienced by polar and temperate diatoms. White dashed lines represent the growth temperatures of the individual cultures..... 26

Figure 15: GAM model predictions of the consecutive flashes before the damping of S-State-induced chlorophyll fluorescence oscillations in polar and temperate diatom cultures over a range of equivalent light levels ($\mu\text{mol photons m}^{-2}\text{s}^{-1}$) at a common measurement temperature of 10°C. The equivalent light levels for the model training data were calculated based on the spacing (seconds) between sequential flashes delivered to the culture..... 27

Figure 16: GAM model predictions of the consecutive flashes before the damping of S-State-induced chlorophyll fluorescence oscillations as predicted by the measurement temperature (°C) and the equivalent light level ($\mu\text{mol photons m}^{-2}\text{s}^{-1}$; with equivalent flash spacings in seconds) experienced by polar and temperate green algae. White dashed lines represent the growth temperatures of the individual strains. 28

Figure 17: GAM model predictions of the consecutive flashes before the damping of S-State-induced chlorophyll fluorescence oscillations in polar and temperate green algae strains over a range of equivalent light levels ($\mu\text{mol photons m}^{-2}\text{s}^{-1}$) at a common measurement temperature of 12°C. The equivalent light levels for the model training data were calculated based on the spacing (seconds) between sequential flashes delivered to the culture. 29

List of Tables

Table 1: Culturing conditions for experimental phytoplankton strains	11
Table 2: Measurement conditions by strain	15
Table 3: Summary statistics by phytoplankton strain of GAM models using the restricted maximum likelihood method to model the response of the damping of S-State-induced chlorophyll fluorescence oscillations to the predictors of deviation from growth temperature (°C) and the equivalent light level ($\mu\text{mol photons m}^{-2}\text{s}^{-1}$).	22
Table 4: Summary statistics by phytoplankton strain of GAM models using the restricted maximum likelihood method to model the response of the damping of S-State-induced chlorophyll fluorescence oscillations to the predictors of measurement temperature (°C) and the equivalent light level ($\mu\text{mol photons m}^{-2}\text{s}^{-1}$).	25

Acknowledgements

First and foremost, thank you to my supervisor, Dr. Campbell. Beyond sharing his guidance and wisdom, he has consistently pushed me to become a better scientist, for which I am endlessly grateful.

Additionally, I would like to acknowledge all the wonderful people who have supported this project. This research would not have been possible without our incredible collaborators at the International Research Laboratory Takuvik at Université de Laval and the Cvetkovska Lab at the University of Ottawa. Likewise, I would like to thank Dr. Dusenge for acting as my committee member and second reader. Further, I am immensely grateful to the members of the Campbell Lab- Dr. Maximilian Berthold, Dr. Sylwia Sliwinska-Wilczewska, Naaman Omar, Mireille Savoie, and Miranda Corkum- for their help and kindness.

Throughout my time at Mount Allison, the care and encouragement shown by my peers, professors, and lab instructors have been outstanding. I feel exceptionally fortunate to have been part of such an extraordinary community. To my family, friends, and honours cohort, thank you for your unwavering support throughout my honours project.

Lastly, I would like to acknowledge the Latitude and Light NSERC Discovery Grant awarded to Dr. Campbell, which provided funding for this project.

Abstract

Polar phytoplankton are vital to global aquatic ecosystems, driving primary production, biogeochemical cycling, carbon sequestration, biodiversity, and climate regulation. Polar phytoplankton's slow but significant productivity at exceptionally low light suggests possible adaptations for low-light photosynthesis. Yet, the functioning of

We hypothesized that maintaining photosynthesis under extremely low light involves suppressing energetically wasteful charge recombinations in Photosystem II. These recombinations desynchronize the four-step cycle of Photosystem II oxygen evolution. We used single turnover variable chlorophyll fluorescence to detect changes in recombination in polar diatoms and green algae in response to temperature and photon delivery spacing. Prolonged synchronous cycling indicates fewer wasteful recombination reactions and, thus, more efficient photosynthetic energy conversion under low light. We observed that higher photon delivery rates and colder temperatures result in less recombination within taxa. Further, polar taxa synchronized cycles for longer durations than temperate taxa under comparable conditions. Our findings support our hypothesis that diverse polar phytoplankton have evolved capacities to suppress energetically wasteful charge recombinations and sustain photosynthesis under extremely low light. This research challenges the conventional understanding of the limits on photosynthesis under light limitation, helping unravel polar ecosystem dynamics and predict their ecosystem responses to climate change.

Introduction

Polar Phytoplankton

Phytoplankton are photosynthetic microorganisms with diverse evolutionary histories and ecologies. Dominating aquatic environments in biomass, organism abundance, and diversity, phytoplankton are found across oceans, lakes, rivers, streams, estuaries, and wetlands [1].

Photolithotrophic growth, a defining characteristic of phytoplankton, fuels biomass production by harnessing light energy to oxidize inorganic compounds containing carbon, nitrogen, phosphorus, sulphur, and other essential micronutrients [2]. Photosynthetically active radiation (PAR) decreases with depth as the light passing through the water column is scattered and absorbed [3]. Therefore, with photons as the sole energy input, phytoplankton growth is constrained to the photic zone, the region of water receiving sufficient light for photosynthesis. Eventually, light attenuates to a level defined as the bottom limit of the photic zone, operationally established at 1% of surface irradiance, equivalent to 2-20 $\mu\text{mol photons m}^{-2} \text{ s}^{-1}$ [2].

Light availability is further constrained in polar regions, presenting unique challenges for phytoplankton growth [4,5]. Solar angle, sea ice thickness, and snow depth limit the radiation penetrating the ice [6]. The solar elevation angle changes because of Earth's obliquity, or tilt, as it orbits the sun, resulting in the polar night and midnight sun, depending upon latitude and season. The thickness of the ice and snowpack further constrains light, with reflective and relatively opaque ice and snow cover limiting the light passing through to the water below [4]. Snow, in particular, shows high light attenuation properties, further lowering the already limited light energy [5].

Despite these constraints, certain psychrophile phytoplankton demonstrate slow but significant productivity under the ice in the winter through photosynthesis at extremely low light levels [4,5]. Across the Arctic, phytoplankton have been reported beneath the sea ice from Resolute Bay to the North of Svalbard, Baffin Bay, and the Greenland, Barents, Laptev, and Chukchi Seas [7]. In 1995, the lower limit of the photic zone was reconsidered as benthic microalgae in the Antarctic were reported photosynthetically active at light levels less than 1 $\mu\text{mol photons m}^{-2} \text{ s}^{-1}$ [8]. Moreover, more recent studies have documented winter phytoplankton productivity below >1m of snow and 1 m of sea ice, corresponding to PAR below 0.15 μmol

photons $\text{m}^{-2} \text{s}^{-1}$ [5]. This represents photosynthesis occurring at light levels 1-2 orders of magnitude below the traditional lower limit for the photic zone.

Slow but significant growth during winter under the ice underscores the ability of psychrophilic phytoplankton to maintain intact photosystems throughout the polar night [4]. Further, it offers support for a theoretical minimum light level for phytoplankton growth of $0.01 \mu\text{mol photons m}^{-2} \text{s}^{-1}$ [2]. Such low-light phytoplankton photosynthesis and growth may serve to mitigate cell mortality in the extended darkness of winter, establishing a seeding population for the spring bloom [4].

Arctic Blooms

As the ice begins to retreat in the spring, phytoplankton blooms start to appear in the Arctic Ocean. Spring blooms are a major source of annual net primary production in this region, representing the most significant event for carbon export to higher trophic levels or biological sequestration in the deep ocean [7]. However, the ice-free period is also characterized by the stratification of surface water, which limits the inorganic nutrient supply [6]. Nutrient limitation imposes an upper limit on the size and duration of polar spring blooms, resulting in a short productive period [6]. Regardless, spring phytoplankton blooms in the Arctic play key global biogeochemical roles in primary production and carbon cycling.

Polar regions play a pivotal role in carbon cycling, representing almost half of the global CO_2 sequestration through microbial photosynthesis [9]. As part of this carbon cycle, phytoplankton form the biological carbon pump, mediating the drawdown of atmospheric carbon to the ocean's interior [1]. The increased solubility of CO_2 at low water temperatures leads to substantial carbon sequestration through deep water formation at the poles, establishing a crucial carbon export pathway from surface waters to the deep ocean [5,7]. Further, substantial CO_2 sequestration arises from high river inputs and the resistance to degradation of the terrestrially derived dissolved organic matter entering the Arctic basin [10].

Phytoplankton are highly productive relative to their biomass, owing to their rapid proliferation and photosynthetic activity in all cells, which distinguishes them from terrestrial plants [1]. This productivity supports rapid consumption by higher trophic levels, creating a prolific food source for ice-associated zooplankton and amphipods. Therefore, the timing of spring blooms is crucial in shaping food availability and the hatching success of associated

zooplankton [5]. As the base of polar food webs, changing phytoplankton dynamics can have repercussions across all trophic levels.

The dynamics of polar phytoplankton blooms are currently undergoing substantial changes in both total annual productivity and seasonal peaks, primarily driven by climate change [7,11]. In the Arctic, the pace of warming is accelerating, resulting in multifaceted alterations within the marine ecosystem. The warming-induced reduction in sea ice extent and thickness has increased light availability, extending the potential phytoplankton growing season and expanding their potential open-water habitats [7]. Simultaneously, escalating freshwater inputs from melting contribute to an increase in vertical stratification, influencing nutrient availability. However, these effects are counterbalanced by heightened storm frequency and increased wind speeds, fostering vertical nutrient mixing [7]. Further, ocean acidification results in reduced calcification, while increased water temperatures boost metabolic activity for some species while posing challenges for obligate cold extremophiles [7,12].

These climate-driven modifications extend across the atmosphere, cryosphere, and ocean, and greatly alter marine ecological dynamics, including productivity, interspecific interactions, population mixing, and pathogen and disease transmission [7]. Comprehending the adaptations and ecophysiology of psychrophilic phytoplankton becomes imperative in anticipating the consequences of these rapid global changes.

Cold Adaptations

Numerous adaptations enable some psychrophile phytoplankton to survive in extreme polar environments. Microbes inhabiting sea ice must contend with solar, osmotic, oxidative and nutrient stress [10]. Further, as poikilotherms, they must overcome the severe inhibiting effects of a cold, low-energy environment. Cold temperatures place severe physiochemical constraints on the cellular functions of psychrophile phytoplankton, exerting a negative influence on water viscosity, solute diffusion rates, membrane fluidity, enzyme kinetics and macromolecule interactions [10].

As a result of their extreme environments, certain psychrophilic phytoplankton exhibit high genetic divergence from closely related temperate species. A study of the polar diatom *F. cylindrus* found that approximately 25% of its genome consists of loci with highly divergent alleles from their mesophilic relatives [13]. Genes related to catalytic activity, transport, metabolic processes and those integral to membranes were shown to be significantly enriched

compared to temperate species, consistent with known microbial adaptations to cold temperatures [13].

To combat the harsh cold, some psychrophiles produce new compounds or alter existing ones. Cryospheric enzyme flexibility is promoted by changes in protein structure, including amino acid substitutions, H-bonds, and salt bridges [10]. Further, synthesizing cold shock proteins minimizes cold protein denaturation while promoting replication, transcription, and translation under low-temperature conditions [10]. Psychrophile phytoplankton also possess anti-freeze proteins (AFPs), encoded by numerous genes identified through metagenomic analyses [14]. AFPs are released into the extracellular space, where they act on ice through an adsorption-inhibition mechanism, effectively inhibiting ice recrystallization. As temperatures dip below freezing, AFPs attach to the ice crystal, forcing the ice front to grow between them. This induces a surface curvature of the crystal that shifts the equilibrium vapour pressure, lowering the local freezing point and limiting local ice growth [14].

Beyond novel compounds, polar microbes alter their cell membranes and solutes. First, they utilize cellular-compatible solutes, including sugars, polyols, amino acids, betaine, and DMSP, which reduce intracellular freezing points and maintain enzyme hydration spheres, stabilizing catalytic activity [10]. Additionally, they exhibit high levels of polyunsaturated fatty acids (PUFAs) in their lipid membranes, including cell membrane phospholipids and chloroplast membrane galactolipids [10,12]. The unsaturated bonds contribute to a looser packing of lipids, maintaining membrane fluidity at cold temperatures.

Moreover, many psychrophilic species coordinate multiple metabolic routes to achieve photostasis, a delicate balance between energy input and utilization [12]. During dark periods, they employ the Entner-Doudoroff pathway (EDP). While the EDP provides less energy per molecule of glucose than glycolytic metabolism, it requires fewer resources for enzyme synthesis, representing a strategic trade-off [15]. Using this alternate metabolism may help the phytoplankton to retain the functionality of their photosynthetic apparatus during prolonged dark periods, allowing them to quickly recover upon re-illumination [12].

Much is known about these diverse physiochemical adaptations for surviving cold temperatures and low light. However, possible bioenergetic adaptations in the photosynthetic apparatus of psychrophilic phytoplankton remain understudied.

Energetic Principles of Photosynthesis

Oxygenic photosynthesis is the metabolic process by which light energy, water, and carbon dioxide are converted to oxygen and carbohydrates. Photosynthesis in eukaryotic phytoplankton occurs in specialized organelles called chloroplasts, which are bound by a two-to-four-membrane envelope, depending upon taxa, and filled with a granular matrix called the stroma [3]. The stroma comprises a concentrated solution of proteins, including the enzymes used in carbon dioxide fixation. Within the stroma are thylakoids, membranes containing pigments and electron carriers. The thylakoid membrane is composed of a polar lipid bilayer, and embedded in it is photosystem II (PSII), a multi-subunit protein complex (Figure 1) [3,16].

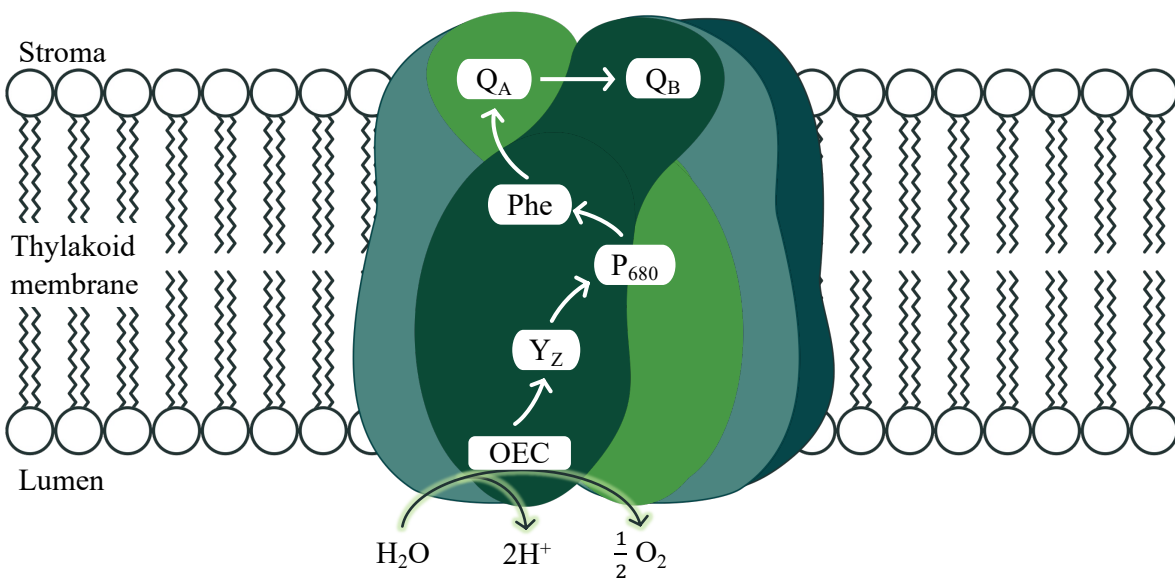


Figure 1: Electron flow through the photosystem II protein complex within the thylakoid membrane of chloroplasts.

PSII consists of 17 transmembrane protein subunits, three membrane-extrinsic protein subunits, and more than 40 cofactors, including the Mn cluster, chlorophylls, carotenoids, plastoquinones, and Fe²⁺, Ca²⁺, and Cl⁻ ions [17,18]. During photosynthesis, PSII catalyzes light-induced charge separation and water oxidation, transferring electrons from a donor to acceptor molecules and producing molecular oxygen [3].

In PSII, photons are captured by light-harvesting chlorophyll molecules, composed of a central magnesium atom surrounded by cyclic tetrapyrrole [3]. Absorption of a photon by a chlorophyll molecule initiates a transition from the ground state to an electrically excited state. The excitation energy is distributed variably among three pathways: photochemistry, dissipation

as heat (non-photochemical quenching, NPQ), and re-emission as fluorescence (ChlF) [19]. Energy directed towards photochemistry by antenna pigments first undergoes rounds of inductive resonance transfer among multiple pigments before eventually reaching the reaction center of PSII, where actual photochemistry occurs [3]. The reaction center, P_{680} , is composed of a Chl a heterodimer P_{D1} and P_{D2} [18,20].

When P_{680} is raised to its excited state, P_{680}^* , it transfers an electron to an initial acceptor molecule, thereby photooxidizing to P_{680}^+ , which then withdraws an electron from a donor molecule [3]. On the acceptor side, P_{680}^+ first passes an electron to pheophytin (Phe). The electron from reduced Phe is transferred to plastoquinone A (Q_A), followed by transfer to plastoquinone B (Q_B) [18]. Once Q_B is fully reduced by receiving two electrons, the reduced Q_B is released, carrying the electrons into the mobile plastoquinone pool in the lipid phase of the thylakoid membrane [3]. On the donor side, P_{680}^+ returns to its ground state P_{680} by taking an electron from a tyrosine residue D1-Tyr-161 (Y_z). Y_z , in turn, extracts an electron from the manganese cluster in PSII [21].

Recombination

During photosynthesis, electron transfers occur at both the donor and acceptor sides of Photosystem II (PSII), stabilizing separated charges [18]. However, these reactions remain reversible, occasionally resulting in the backflow of electrons through the pathway, referred to as recombination reactions [22]. Recombination plays a pivotal role in photodamage and photoprotection, harming PSII but proving essential for survival under excess light conditions [23].

At elevated light levels, the prior reduction of downstream electron acceptors blocks electron transfer from P_{680}^* . Under such conditions, the primary radical pair [$P_{680}^+Phe^-$] will recombine, generating the excited triplet chlorophyll $^3P_{680}$ (Figure 2) [24]. Chlorophyll triplets react with ground-state molecular oxygen to produce singlet oxygen (1O_2), a highly damaging, photoinhibitory reactive oxygen species [23].

Conversely, non-radiative charge recombination acts as a mechanism of photoprotection [18]. These pathways enable direct recombination from the singlet $P_{680}^+Phe^-$ or $P_{680}^+Q_A^-$ state and are governed by the redox potential of the Q_A and Phe electron acceptors [25]. Direct recombination helps prevent the accumulation of excess energy and competes with triplet

chlorophyll formation in the PSII reaction center, thereby reducing the formation of harmful ROS [22].

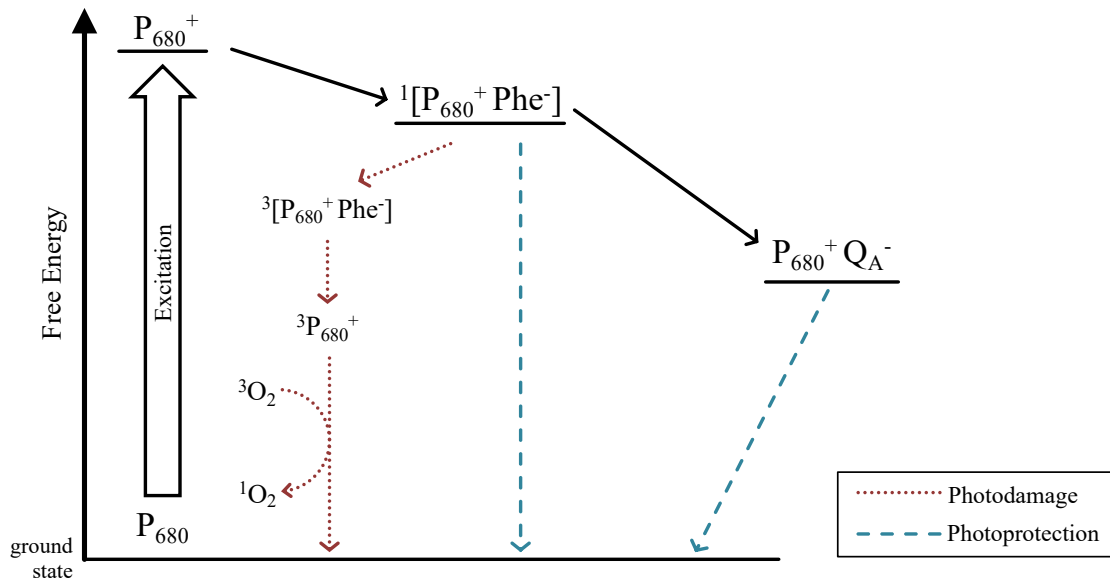


Figure 2: Photodamaging and photoprotective recombination pathways in photosystem II.

Beyond their roles in photodamage and photoprotection, charge recombination reactions may also occur as a wasteful process that lowers photosynthetic energy conversion efficiency [23]. Altering reduction potentials of downstream electron acceptors, leading to changes in energy gaps, may represent evolutionary adaptations aimed at maximizing photoprotection and minimizing inefficient back-reactions under light-limited conditions [26].

S-State Cycling

The oxygen-evolving complex (OEC) of PSII is the active site where water is converted to oxygen and protons [27]. It consists of a metal-oxo cluster with the formula Mn_4CaO_5 . As P_{680} absorbs successive photons, they induce charge separations, which cause electrons to be extracted from the Mn cluster. Each electron removed from the WOC replaces one lost by the reaction center when an electron is transferred downstream to metabolism. Consecutive charge separations induce four increasingly oxidized states, known as S-States [28], denoted as S_0 , S_1 , S_2 , and S_3 , followed by a transient S_4 state, which rapidly decays to S_0 (Figure 3). Once four photons have been absorbed and the Mn cluster has lost four electrons, it replaces them by oxidizing two water molecules to one molecule of molecular oxygen. Therefore, a complete water oxidation cycle during oxygenic photosynthesis requires the sequential

complete water oxidation cycle during oxygenic photosynthesis requires the sequential absorption of four photons by a PSII, with the progressive accumulation of four oxidizing equivalents in the OEC [27–29].

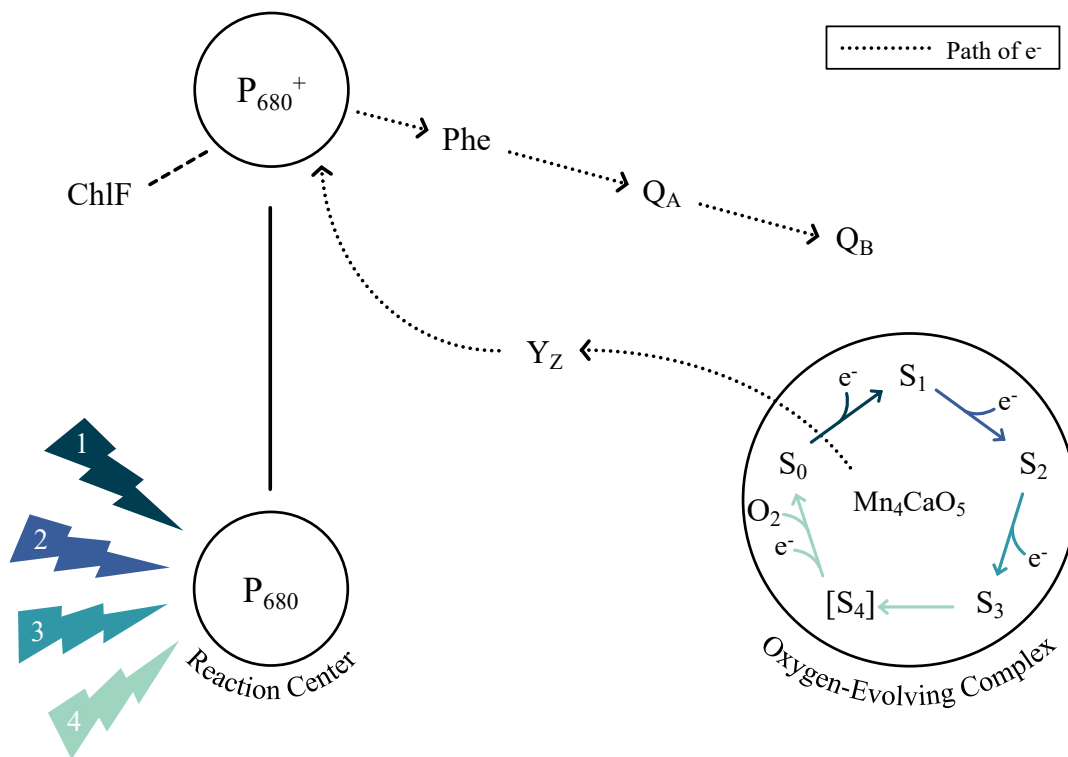


Figure 3: Pathway of S-State cycling and the electron transfer in PSII. Successive PSII charge separations extract successive electrons from the Mn cluster, inducing four increasingly oxidized states. After accumulating four oxidizing equivalents, 2 H_2O molecules are oxidized to 1 O_2 and four protons released to the luminal side of the thylakoid.

Stable S-State cycling allows cells to maintain productive photosynthesis under light limitation, characterized by widely spaced photon arrivals. With low PSII excitation rates, there is less pressure driving downstream electron flow [30]. Under these conditions, there is an elevated probability of energetically wasteful recombination reactions, representing a step backward in the S-State cycle [30,31]. However, stable S-State cycling under low light ensures continued electron flow through the ETC, sustaining ATP and NADPH production, and minimizing the risk of photodamage to the photosynthetic machinery [23,30].

Study Aims

This study evaluates if psychrophilic diatoms and green algae have evolved to increase photosynthetic energy conversion efficiency by maintaining stable S-State cycling and productive electron transport under low light, by minimizing inefficient back reactions.

The stability of S-State cycling in a phytoplankton sample may be evaluated by the applications of sequences of short, very bright, single-turnover light flashes. As sequential light flashes are applied, the population of PSII is driven synchronously through the S-State cycle [29]. In an idealized sample, the four S-States will be reflected by an ongoing periodic oscillation in ChlF. However, recombination reactions represent a loss of charge separation and wasteful slippage in the S-State cycling of individual PSII. As more recombination events occur, desynchronization of S-State cycling among the PSII of the population will scramble the periodic changes in ChlF, dampening the observed oscillation [31]. An organism exhibiting S-State cycling over more flash cycles indicates fewer inefficient back reactions and potentially more efficient photosynthetic energy conversion.

By comparing the S-State cycling over flash cycles, of psychrophilic and temperate taxa, we can determine if psychrophilic diatoms and green algae have evolved increased photosynthetic efficiency and under what conditions they may have a significant advantage in stable extraction of electrons from water.

Materials & Methods

Study Strains

Seven phytoplankton species were studied, including polar and temperate strains of diatoms and green algae. *Fragilariopsis cylindrus*, a psychrophilic pennate diatom measuring 15-55 μm , thrives in the high salinity and subzero temperatures of Arctic and Antarctic sea-ice systems [32,33]. Forming large blooms in the bottom layer of sea ice and across the wider sea ice zone, *F. cylindrus* acts as a keystone and indicator species for polar ecosystems [32,34]. Conversely, *Thalassiosira pseudonana* is a small (2.5-15 μm) centric diatom found worldwide in diverse freshwater, coastal, brackish, and marine habitats [35]. *T. pseudonana* can tolerate a wide range of salinities (0.5%–37%) and temperatures (4–25°C), contributing to its frequent use as a model diatom species [35].

Chlamydomonas ICEMDV and *Chlamydomonas priscuii* are halotolerant algae isolated from the perennially ice-covered hypersaline Lake Bonney, in McMurdo Dry Valleys, Antarctica [36,37]. With large (15 to 20 μm) biflagellate cells, *C. ICEMDV* dominates the shallow photic zone, where it experiences higher irradiance, extreme nutrient limitation, and lower salinity [36,38]. The smaller *C. priscuii* dominates the deep photic zone, characterized by permanent low temperatures, low irradiance, and high salinity [12,39]. The final psychrophile species is *Chlamydomonas malina*, a marine microalga isolated from the Arctic Ocean's Beaufort Sea, measuring around 10 μm in length and 5 μm in width, and growing optimally at 4°C [40,41]. The temperate *Chlamydomonas reinhardtii* is a model green alga approximately 10 μm in size and found in soil and aquatic environments with an optimal temperature range of 20-32°C [42,43]. Further, *Chlorella vulgaris*, ranging from 2 μm to 10 μm in size, is primarily found in freshwater environments and grows optimally at 27°C [44,45].

Culturing Protocols

The seven species and their respective culturing conditions are summarized in Table 1. Cultures of *T. pseudonana* and *C. vulgaris* were prepared by Naaman Omar (Mount Allison University); *Chlamydomonas* cultures were prepared by MacKenzie Poirier (Cvetskova Lab, University of Ottawa); and *F. cylindrus* cultures were prepared by Sébastien Guérin (Takuvik International Research Laboratory, Université Laval).

Table 1: Culturing conditions for experimental phytoplankton strains

Genus	Species	Growth Temp (°C)	Par ($\mu\text{mol photons m}^{-2}\text{s}^{-1}$)	Photoperiod	Media
<i>Thalassiosira</i>	<i>pseudonana</i>	22	50	12	F2
<i>Chlorella</i>	<i>vulgaris</i>	22	50	12	F2
<i>Chlorella</i>	<i>vulgaris</i>	22	50	12	BG11
<i>Chlorella</i>	<i>vulgaris</i>	22	70	12	BG11
<i>Thalassiosira</i>	<i>pseudonana</i>	22	70	12	F2
<i>Fragilariopsis</i>	<i>cylindrus</i>	0	10	24	F2
<i>Fragilariopsis</i>	<i>cylindrus</i>	6	10	24	F2
<i>Chlamydomonas</i>	<i>priscuii</i>	4	10	24	BBM
<i>Chlamydomonas</i>	<i>ICEMDV</i>	4	10	24	BBM
<i>Chlamydomonas</i>	<i>malina</i>	4	10	24	BBM
<i>Chlamydomonas</i>	<i>reinhardtii</i>	24	10	24	BBM

Single Turnover Variable Chlorophyll Fluorescence

A single turnover variable chlorophyll fluorescence (St-ChlF) approach was employed to evaluate the progressive desynchronization of the S-State cycle across the range of phytoplankton species and growth temperatures.

A 100 μL sample of each culture was taken for a chlorophyll assay. Chlorophyll was extracted using a solution of acetone and DMSO over a 30-minute period in darkness, and concentrations were measured using a Trilogy Laboratory Fluorometer (Turner Designs).

Then, 3 mL samples of culture were loaded into a temperature-controlled cuvette (PolyScience) placed within the measurement chamber of a Soliense LIFT-REM fluorometer (Version LIFT-REM 1.0, Soliense Inc). The apparatus was covered to block out incident light and cells were acclimated to the dark for a minimum of 30 seconds. In a dark regulated state, non-photochemical quenching processes are relaxed, and electrons have been passed downstream from all PSII centres, leaving all PSII reaction centres in ground state open for photochemistry upon receipt of an incident photon. Therefore, when a PSII receives a photon, the maximum proportion of energy will be partitioned to photochemistry, corresponding to minimum ChlF (F_0) [19].

The sample is then exposed to a series of 32 short, high-intensity, evenly spaced flashes of 445 nm light. Depending upon the spacing between sequential flashes, each flash series occupied 62 to 542 seconds. Flash series were applied with different spacings, and at different

temperatures, with the culture sample replaced for each new measurement temperature. Each flash consists of a rapid series of 50-70 sub-saturating flashlets of 1.6 μs , delivered every 4.1 μs , over a total of 205 - 287 μs [19]. These flashlets induce the absorption of light by PSII, which then passes an electron downstream to Q_A^- , effectively closing PSII for photochemistry over a period of $\sim 1000 \mu\text{s}$ [29,46]. Closing the photochemistry pathway redirects a greater proportion of additional incoming light energy to ChlF, resulting in maximum ChlF (F_m). This induction is known as the saturation phase (Figure 4), where the fluorescence yield increases from a minimum (F_o) to a maximum (F_m) [47]. For each flash, the ChlF minima and maxima are extracted using a fitting model (LIFT software version 22.11.11, Soliense Inc) [48]. F_o and F_m can then be used to derive the maximum quantum yield of photochemistry in PSII, a secondary ChlF parameter calculated as follows [19]:

$$F_v/F_m = \frac{F_m - F_o}{F_m} \text{ (Equation 1)}$$

The maximum quantum yield represents the efficiency with which an open PSII can convert absorbed light energy into chemical energy.

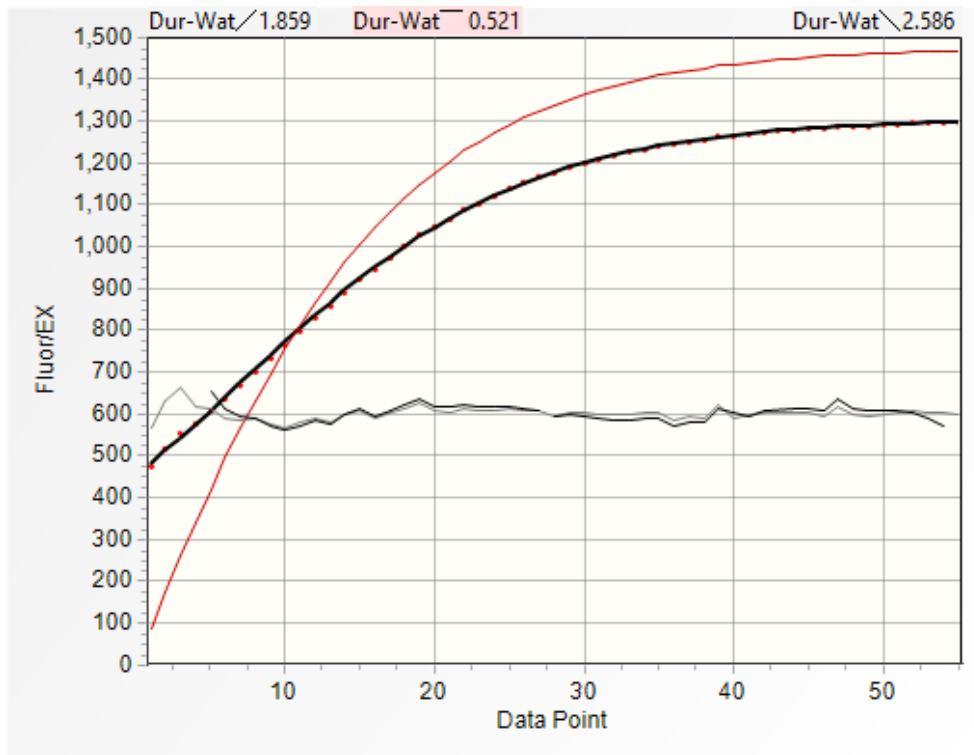


Figure 4: Sample chlorophyll fluorescence induction curve

The brightness of the flashes and the number of sub-saturating flashlets required for full saturation varies between cultures. These experimental parameters depend on the effective absorption cross-section of photosystem II (σ_{PSII}), estimated from the ChlF induction curve during the saturation phase [48]. σ_{PSII} represents the probability of light capture by the PSII antenna bed associated with the dark-adapted PSII [19,49]. When σ_{PSII} is larger, weaker or fewer flashes are required to saturate the population of PSII while limiting stress or double turnovers of PSII associated with excess light [49]. Conversely, a small σ_{PSII} requires brighter or more numerous flashlets to ensure that the proportion of closed reaction centres increases progressively to saturation. If the brightness and number of sub-saturating flashlets are appropriate for the culture, the fluorescence will reach a plateau after approximately 70-80% of the flashlets, as depicted in Figure 4 [48].

Each flash is bright enough to deliver, on average, a photon to each PSII, but short enough to limit the probability of a PSII going through two rounds of photochemistry during the flash. Each flash thus advances a transition between S-States for each PSII. Thus, as sequential flashes are applied to the culture, each individual PSII is driven through the four S-States (Figure 5) [29]. As the oxygen-evolving complex of PSII moves between S-States, it alters the system's kinetics and free energy [26]. Since the energy allocated to ChlF is modulated by the energy allotted to photochemistry and thermalization, the yield of ChlF varies between S-States [19,27].

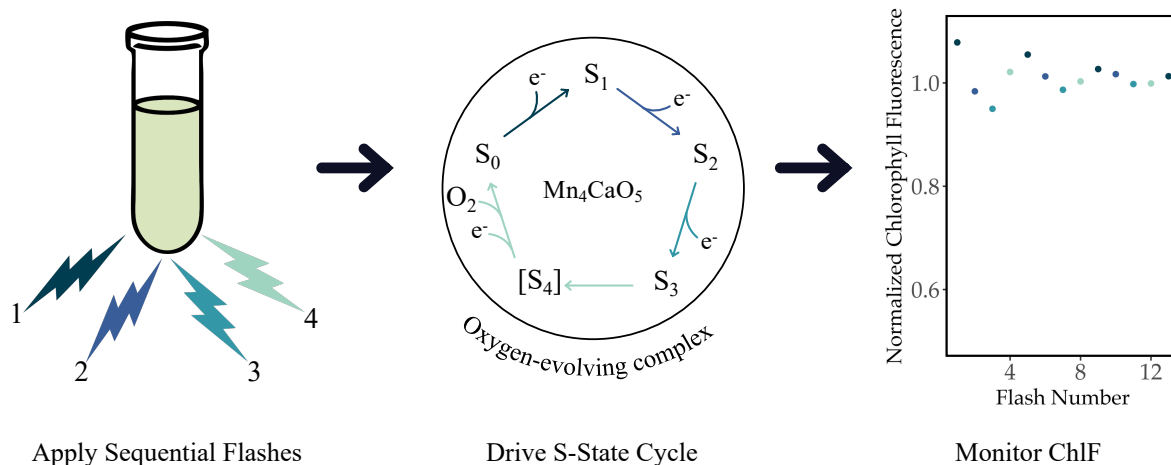


Figure 5: Repeated single-turnover excitation of variable chlorophyll fluorescence for monitoring the S-State cycling in PSII during photosynthesis. Sequential flashes drive S-State transitions from S₀ to S₁, S₁ to S₂, S₂ to S₃, and S₃ to the transient S₄ state, which rapidly decays to S₀.

In an idealized culture, the population of PSII will cycle synchronously, reflected by an ongoing oscillation in chlorophyll fluorescence with a period of four (Figure 5) [31]. However, a recombination reaction, representing the loss of charge separation, will cause a missed step in the S-State cycling of an individual PSII. As more recombination events occur, desynchronization of S-State cycling among the population of PSII will scramble the periodic changes in ChlF, dampening the observed oscillation of the population-level fluorescence [31]. Prolonged synchronous cycling thus reflects fewer wasteful recombination reactions at the level of each PSII and thus, more efficient photosynthetic energy conversion.

Measurement Conditions

By evaluating the S-State cycling of polar and temperate taxa of diatoms and green algae under a range of equivalent light levels and measurement temperatures (Table 2), we can determine if polar taxa have evolved to increase photosynthetic energy conversion efficiency by minimizing inefficient recombination reactions.

Measurement temperatures ranged from 0 to 28°C, depending on the taxa (Table 2). While light absorption and energy transfer within PSII are not temperature-sensitive, the redox reactions associated with downstream electron transport are highly temperature-dependent [39]. Notably, the incidence of charge recombination typically decreases with temperature [50]. However, this effect may be minimized in strains possessing adaptive mechanisms to regulate photosynthetic electron flow, S-State transitions, and energy partitioning [39]. Thus, comparing S-State cycling across measurement temperatures helps unravel the properties of the photosynthetic apparatus.

Altering the spacing between sequential flashes can simulate varying equivalent light conditions. At higher light levels, more photons arrive per unit of time, corresponding to shorter spacing between saturating flashes in our measurement protocol (Figure 5). Cultures were evaluated at flash spacings of 1, 2, 4, 8, and 16 seconds. The equivalent light levels are estimated using the σ_{PSII} for each unique measurement condition as follows:

$$\text{Light}(\mu\text{mol photons m}^{-2}\text{s}^{-1}) = \frac{1}{\text{flash spacing (s)}} \times \frac{1}{\sigma_{\text{PSII}}(\text{\AA}^2 \text{ photon}^{-1})} \times \frac{1\text{m}^2}{1\text{E}20\text{\AA}^2} \times \frac{1 \mu\text{mol}}{6.02 \text{ 2E}17 \text{ photons}} \quad \text{(Equation 2)}$$

The conversions of flash spacing to light levels yielded similar ranges of equivalent measurement light levels for each strain (Table 2). For comparison, full sunlight at the sea surface is $\sim 2000 \mu\text{mol photons m}^{-2}\text{s}^{-1}$, so our measurement light ranges are ~ 5 orders of magnitude lower than full sunlight, and ~ 2 -3 orders of magnitude below the $\sim 20 \mu\text{mol photons m}^{-2}\text{s}^{-1}$ threshold, used to define the conventional bottom of the photic zone supporting photosynthetic productivity in the oceans [2].

Table 2: Measurement conditions by strain

Strain	Flash Spacings (s)	Steady Light Levels ($\mu\text{mol photons m}^{-2}\text{s}^{-1}$)	Measurement Temperatures ($^{\circ}\text{C}$)
<i>F. cylindrus</i>	1, 2, 4, 8, 16	0.02981 - 0.65678	0, 2, 6, 10
<i>T. pseudonana</i>	1, 2, 4, 8, 16	0.02428 - 0.53428	10, 14, 18, 20, 22, 24, 28
<i>C. ICEMDV</i>	1, 2, 4, 8, 16	0.04252 - 0.73733	4, 8, 12
<i>C. priscuii</i>	1, 2, 4, 8, 16	0.04289 - 0.77084	4, 8, 12
<i>C. malina</i>	1, 2, 4, 8, 16	0.03705 - 0.65817	4, 8, 12
<i>C. reinhardtii</i>	1, 2, 4, 8, 16	0.04670 - 0.84377	12, 16, 20, 24
<i>C. vulgaris</i>	1, 2, 4, 8, 16	0.05102 - 0.89781	10, 14, 18, 22, 26

Analytical Methods

Data was processed using R version 4.3.2 and RStudio version 2023.12.0+369 on the x86_64-apple-darwin20 (64-bit) platform and running under macOS Sonoma 14.3.1. Fluorescence data files generated by LIFT software were imported, tidied, and combined with metadata on each culture using the tidyverse [51], lubridate [52], and googlesheets4 [53] packages. The tidyverse, doBy [54], and WaveletComp [55] packages were used for wavelet analyses. Lastly, the mgcv [56] and mgcViz [57] packages were used for generalized additive modelling, while the ggplot2 [58] and metR [59] packages were used for data visualization.

Wavelet Transformations

The fluorescence data yields a time series of F_v/F_m over 32 flashes for each flash spacing and each measurement temperature, for each culture sample. The fluorescence time series were analyzed for each combination of strain, growth conditions, measurement temperature, and flash spacing, using wavelet transformations [60], as exemplified in Figure 6. Unlike traditional methods, wavelet analysis does not assume that the statistical properties of a time series are

constant. Instead, wavelet transformations locally decompose the signal across different time scales and estimate spectral characteristics as a function of time [61]. By examining the frequency and wavelet power spectra, we can uncover the dominant patterns in the data [60].

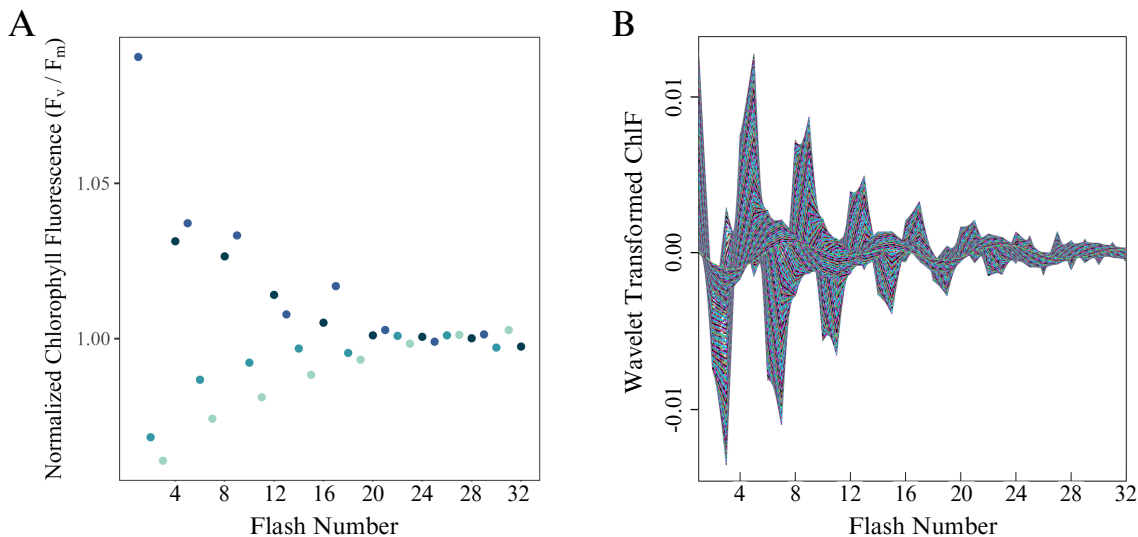


Figure 6: Representative wavelet transformation of *Chlamydomonas priscuii* fluorescence over 32 consecutive flashes, measured at 4°C and 1-second flash spacing, equivalent to a photon delivery rate to PSII achieved under an equivalent light level of $0.708 \mu\text{mol photons m}^{-2} \text{s}^{-1}$.

The core of the wavelet transformation involves computing the wavelet power spectrum of the standardized time series using the Morlet wavelet [60]. Further, the statistical significance of the periodic components in the time series was calculated using a simulation algorithm. Surrogate time series are generated based on a white noise model, consisting of uncorrelated random values with constant mean and variance. Comparing the wavelet of the original data with the white noise model, p-values are calculated to determine whether the observed periodic components are statistically significant [60].

The statistical significance of the wavelet power at a periodicity of four indicates whether the culture is exhibiting the periodic oscillations in chlorophyll fluorescence that indicate synchronous S-State cycling across the PSII population. For wavelets exhibiting S-State cycling, we generated a reconstruction limited to areas with a statistically significant signal, as depicted in Figure 7. Damping of the reconstructed wavelet represents the significance of the signal dropping below the threshold of $p=0.05$. The stability index then represents the number of flashes applied before this damping occurs, indicating how many successive photons are

received by the PSII population before recombination reactions desynchronize the S-State cycle towards randomness across the population.

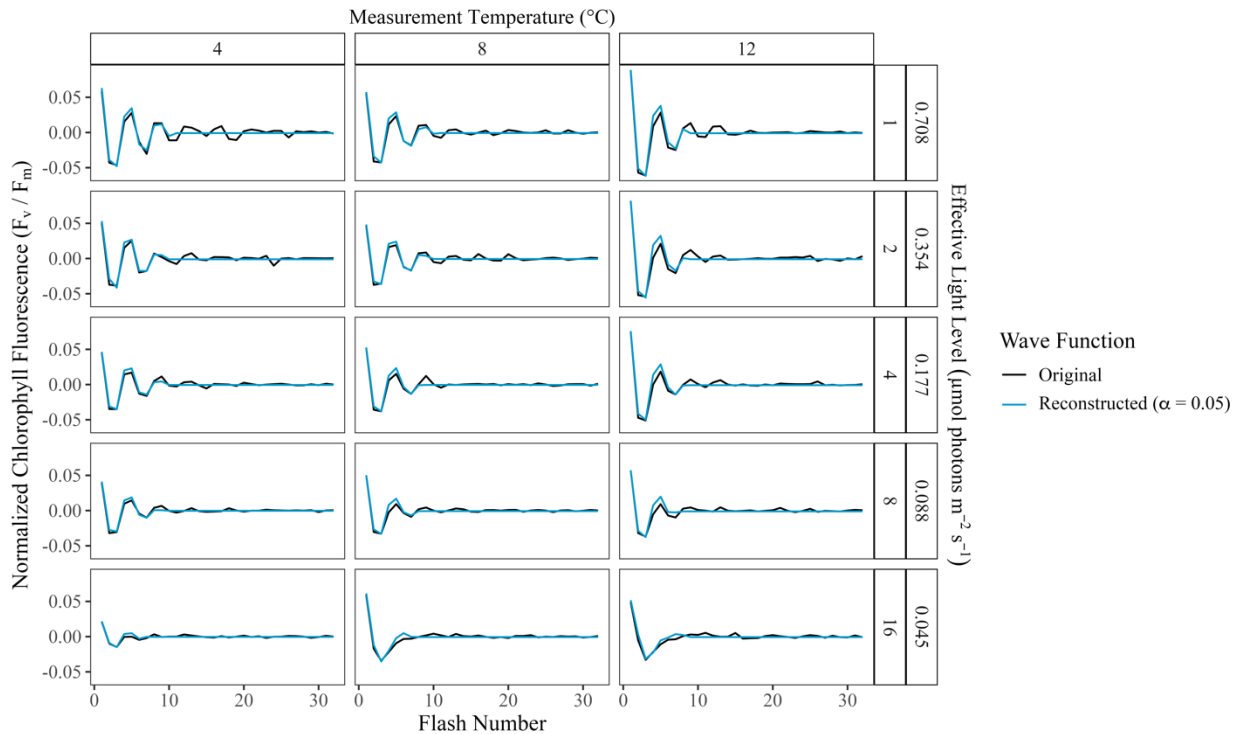


Figure 7: Sample plot illustrating the wavelet reconstructions at $\alpha = 0.05$ of *Chlamydomonas priscuii* fluorescence over 32 consecutive single turnover flashes across a range of measurement temperatures and flash spacings, with their equivalent light levels.

Generalized Additive Modelling

The observed patterns in the persistence of S-State cycling across conditions within taxa were then modelled using the nonparametric method of generalized additive modelling (GAM). GAMs fit a model to predict the stability index based on a tensor product smooth of the two predictors, temperature, and light level. The response variable is linked to the independent variables using a smoothing function, where many localized polynomials are joined to form a piecewise function called a spline [62]. For each strain, two separate GAM models were fit to the data using the restricted maximum likelihood method (REML). Within each model, k represents the number of basis dimensions and te represents the tensor product smooth. The first model examines the response of S-State damping to light level and deviation from growth temperature according to the following equation, where n is the number of distinct levels of temperature deviation evaluated for that strain:

DampingIndex \sim te(TempDiff, LightLevel, k = n, method = REML **(Equation 3)**)

The second examines the response of S-State damping to light level and measurement temperature according to the following equation, where n is the number of distinct levels of temperature measured for that strain:

DampingIndex \sim te(MeasurementTemp, LightLevel, k = n, method = REML **(Equation 4)**)

Models were validated by verifying the choice of basis dimensions (k) and evaluating the residual plots [63]. Based on the fitted models, the stability index can then be predicted for other combinations of temperature and light [64]. These predictions were then visually represented with a contour plot.

Results

Single Turnover Variable Chlorophyll Fluorescence

Exposing phytoplankton cultures to a series of 32 successive flashes produced oscillations in the maximum quantum yield of photochemistry in PSII, as estimated through the secondary chlorophyll fluorescence parameter F_v/F_m . Initially, the majority of the dark-adapted population of PSII is at S_1 , with a smaller fraction at S_0 [27,31]. As shown in Figure 8 for the polar alga *C. priscuii*, the time series of F_v/F_m over successive flashes reveals consistent variations in fluorescence yield as the predominant S-States follow each other across the PSII within the population. However, the amplitude of the ChlF oscillations declines progressively over time, and with wider spacing of sequential flashes, equivalent to decreasing light levels, and is less pronounced at a higher measurement temperature.

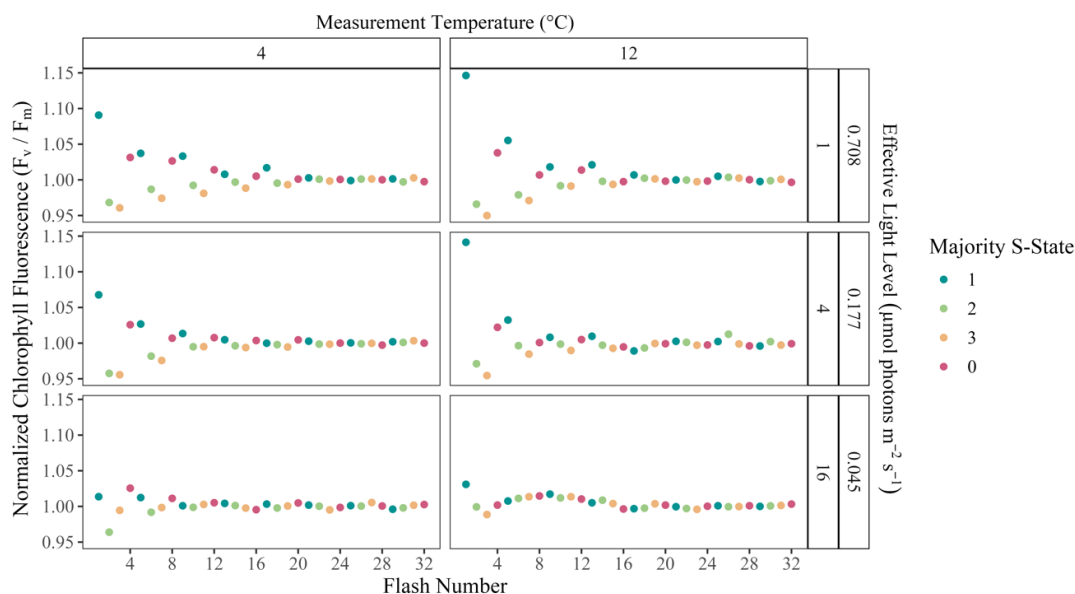


Figure 8: Oscillations in the maximum quantum yield of the photochemistry in *Chlamydomonas priscuii* cultures over a series of 32 flashes, as measured through the secondary chlorophyll fluorescence parameter F_v/F_m . Representative conditions include cultures measured at 4 or 12 °C, with flash spacings of 1, 4, or 16 seconds, equivalent to light levels of 0.045 – 0.708 $\mu\text{mol photons m}^{-2} \text{s}^{-1}$.

Wavelet Analysis

Wavelet transformations were computed for the fluorescence time series of each unique combination of measurement temperature, flash spacing, equivalent to light level, growth temperature, and species or strain. Assessing the wavelet power of a 4-step periodicity across conditions, key trends emerge. As exemplified by the polar alga *C. priscuii* (Figure 9A), the

average wavelet power declines with increasing flash spacings, equivalent to decreasing equivalent light levels, and also with increasing measurement temperatures. While this trend remains in the temperate taxa *C. reinhardtii* (Figure 9B), the wavelet power is consistently lower, suggesting a weaker 4-step periodicity of ChlF in temperate taxa, which is only significant at the shorter flash spacings, with higher equivalent light levels.

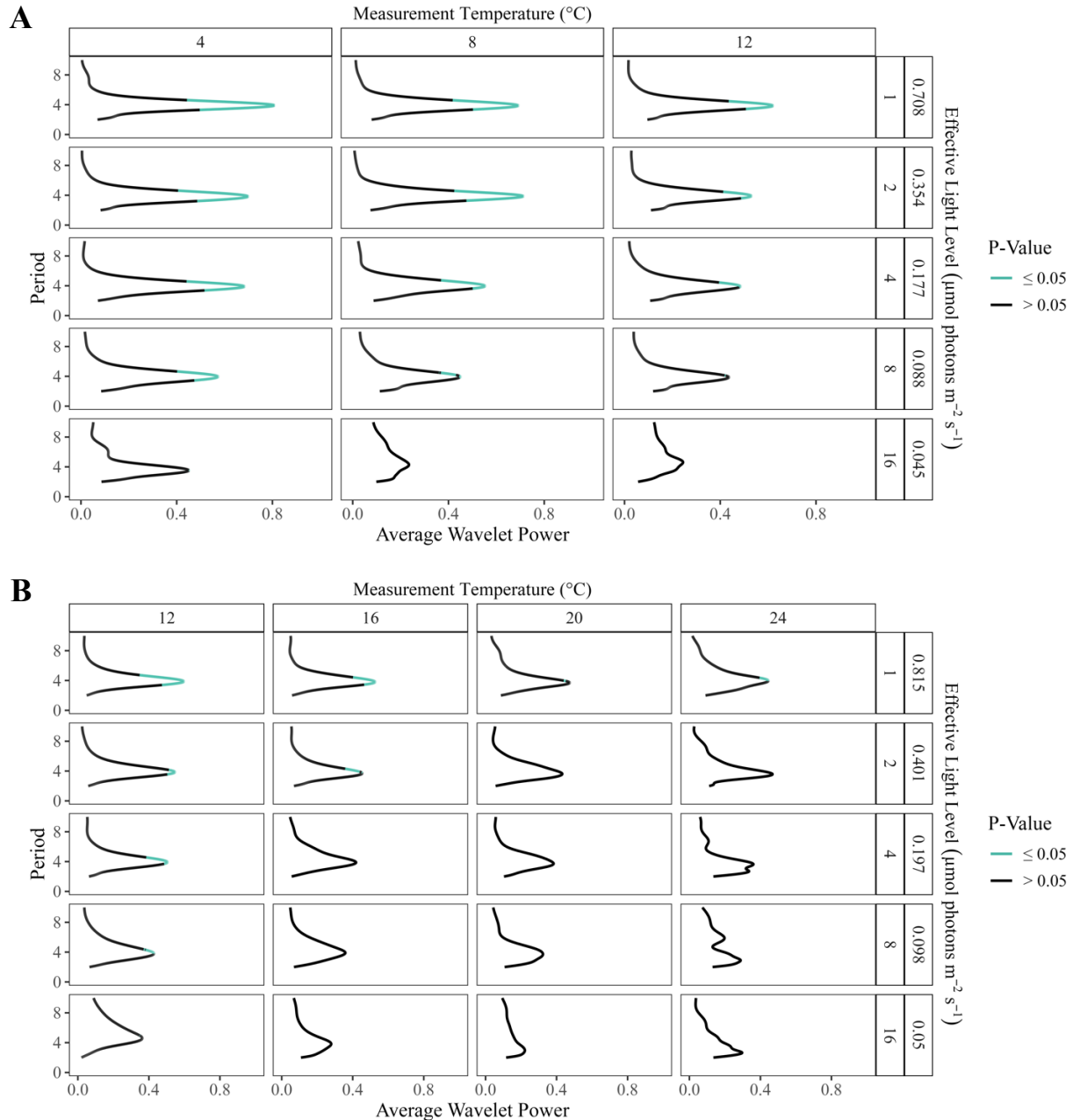


Figure 9: Sample plot of wavelet power by period of oscillations in the maximum quantum yield of photochemistry in A. Polar *Chlamydomonas priscuii* and B. Temperate *Chlamydomonas reinhardtii* cultures across a range of measurement temperatures and flash spacings, with the equivalent light levels.

Polar taxa maintained significant 4-step oscillations in F_v/F_m , and thus stronger synchronization of PSII S-State cycling across a broader range of measurement conditions, than did their temperate counterparts (Figure 10). The temperate diatom *T. pseudonana* showed significant 4-step ChlF oscillations across 20.57 % of measured conditions, compared to 85% of measured conditions in its polar counterpart, *F. cylindrus*. Similarly, significant 4-step ChlF oscillations occurred across 32% and 40 % of measurement conditions for the temperate green algae *C. vulgaris* and *C. reinhardtii*, and 60, 73, and 80% of measurement conditions for the polar algae *C. ICEMDV*, *C. malina*, and *C. priscuii*.

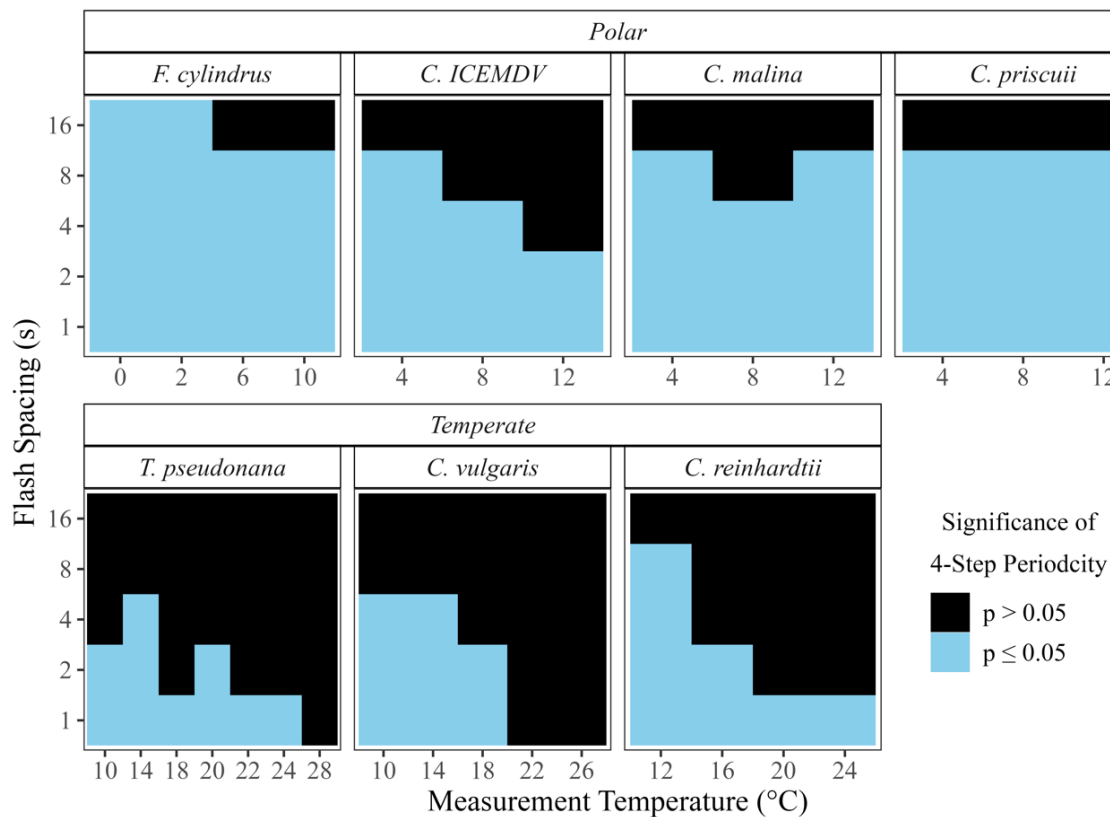


Figure 10: Statistical significance of 4-step oscillations in the maximum quantum yield of PSII photochemistry across polar and temperate phytoplankton taxa, as measured through variable chlorophyll fluorescence.

Generalized Additive Modelling by Deviation from Growth Temperature

Predictions from generalized additive modelling were generated for the damping of S-State-induced chlorophyll fluorescence oscillations, as predicted by the tensor product smooth of the deviation from growth temperature during measurements (°C) and the equivalent light level

($\mu\text{mol photons m}^{-2}\text{s}^{-1}$; Table 3) for each strain. For each model, three summary statistics are generated for the tensor product smooth, an F-ratio, a p-value, and the effective degrees of freedom (EDF), which represents the degree of linearity of the relationship between variables.

Table 3: Summary statistics by phytoplankton strain of GAM models using the restricted maximum likelihood method to model the response of the damping of S-State-induced chlorophyll fluorescence oscillations to the predictors of deviation from growth temperature ($^{\circ}\text{C}$) and the equivalent light level ($\mu\text{mol photons m}^{-2}\text{s}^{-1}$).

Strain	Significance of smooth term			Adjusted R ²	Deviance Explained
	EDF	F-ratio	P-value		
<i>F. cylindrus</i>	7.23	6.82	2.8e-05	0.584	66.1%
<i>T. pseudonana</i>	6.08	9.01	5.38e-06	0.674	73.2%
<i>C. ICEMDV</i>	4.51	6.59	0.00687	0.687	78.8%
<i>C. priscuii</i>	4.31	2.17	0.115	0.389	57.7%
<i>C. malina</i>	4.34	2.56	0.0843	0.423	60.2%
<i>C. reinhardtii</i>	6.05	9.49	0.000274	0.786	85.4%
<i>C. vulgaris</i>	5.39	13.83	4.08e-06	0.772	82.3%

The smoothing term was significant for the polar diatom *F. cylindrus* ($F = 6.835$, $p = 2.8\text{e-}05$), explaining 66.1% (adjusted $R^2 = 0.584$) of the deviance in the stability index. Similarly, the model of the temperate diatom, *T. pseudonana*, produced a significant smoothing term ($F = 9.01$, $p = 5.38\text{e-}06$), which accounted for 73.2% of the deviance in the stability index (adjusted $R^2 = 0.674$). These models were used to predict the number of consecutive flashes before the damping of ChlF oscillations for each strain at each combination of deviation from growth temperature during measurements ($^{\circ}\text{C}$) and equivalent light level ($\mu\text{mol photons m}^{-2}\text{s}^{-1}$; Figure 11).

Both diatom taxa exhibited the longest predicted periodic oscillations in ChlF at higher equivalent light levels and lower temperatures. Notably, the polar *F. cylindrus* sustained cycling longer than its temperate counterpart, *T. pseudonana*, under comparable conditions. This disparity was particularly prevalent above the growth temperature and when longer spacing between flashes produced lower equivalent light levels (Figure 11). Under these conditions, *T. pseudonana* cultures did not retain the significant 4-step oscillation in ChlF indicative of synchronized S-State cycling.

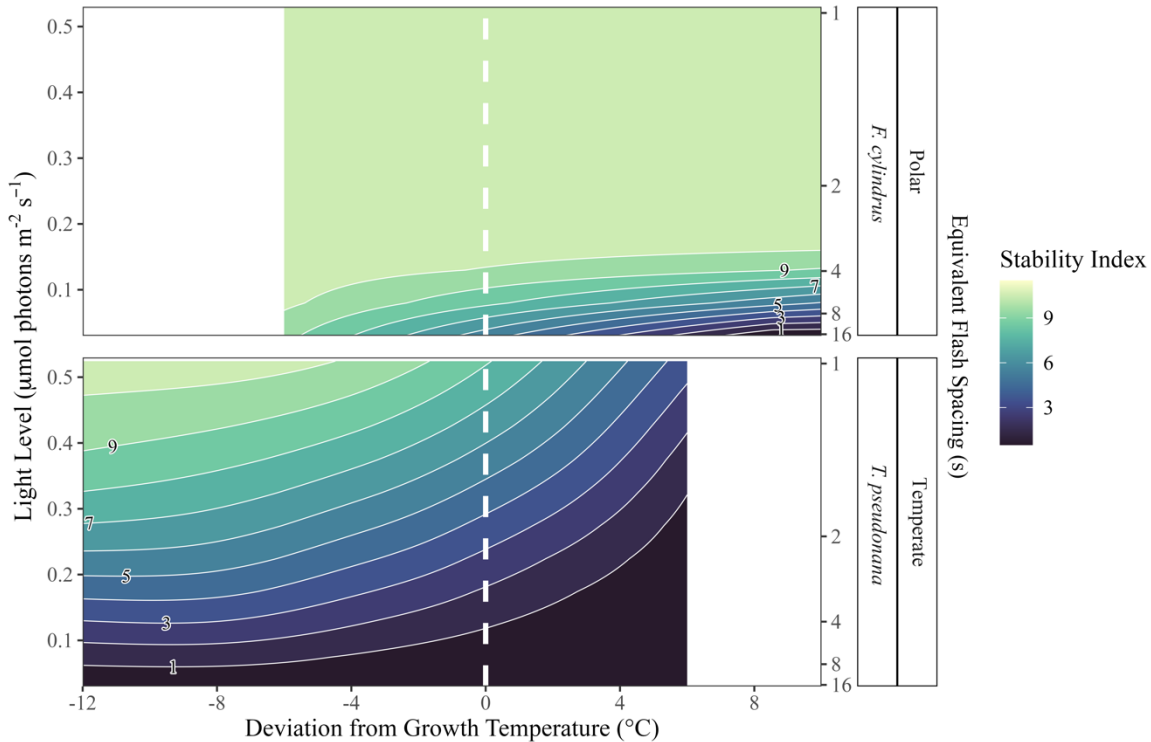


Figure 11: GAM model predictions of the consecutive flashes before the damping of S-State-induced chlorophyll fluorescence oscillations as predicted by the deviation from growth temperature ($^{\circ}\text{C}$) during measurements and the equivalent light level ($\mu\text{mol photons m}^{-2}\text{s}^{-1}$, with flash spacings in seconds) experienced by polar and temperate diatoms. White dashed vertical lines represent the growth temperatures.

The GAM outputs varied more among green algal strains (Table 3). The smoothing term was significant for the temperate strains *C. reinhardtii* ($F = 9.49$, $p = 0.000274$) and *C. vulgaris* ($F = 13.83$, $p = 4.08\text{e-}06$), predicting 85.4% (adjusted $R^2 = 0.786$) and 82.3% (adjusted $R^2 = 0.772$) of the deviance in the stability index, respectively. However, while the smoothing term was significant ($F = 6.59$, $p = 0.00687$), predicting 78.8% (adjusted $R^2 = 0.687$) of the deviance for the polar *C. ICEMDV*, it was not significant for the other two polar taxa. For *C. priscuii*, the statistical evaluation of the smoothing term produced an F value of 2.17 and a corresponding p-value of 0.115, explaining only 57.7% (adjusted $R^2 = 0.389$) of the deviance in the response variable. Similarly, the non-significant smoothing term for *C. malina* ($F = 2.56$, $p = 0.0843$) only explained 60.2% of the deviance in the stability index (adjusted $R^2 = 0.423$).

Overall, model predictions for green algal strains exhibited a similar pattern to the diatoms, with the longest predicted oscillations in ChlF at measurement conditions with higher equivalent light levels (shorter spacing between flashes) and lower measurement temperatures relative to

growth temperature (Figure 12). The trends shown by the three strains of polar algae are remarkably consistent, displaying virtually identical patterns and differing by only 1-2 flashes before signal damping, under identical conditions (Figure 12). Further, much like the temperate diatoms, the temperate algae *C. reinhardtii* and *C. vulgaris* did not exhibit significant periodic oscillations in ChlF at measurement temperatures near or above their growth temperature and under the low light conditions produced by longer flash spacings (Figure 12).

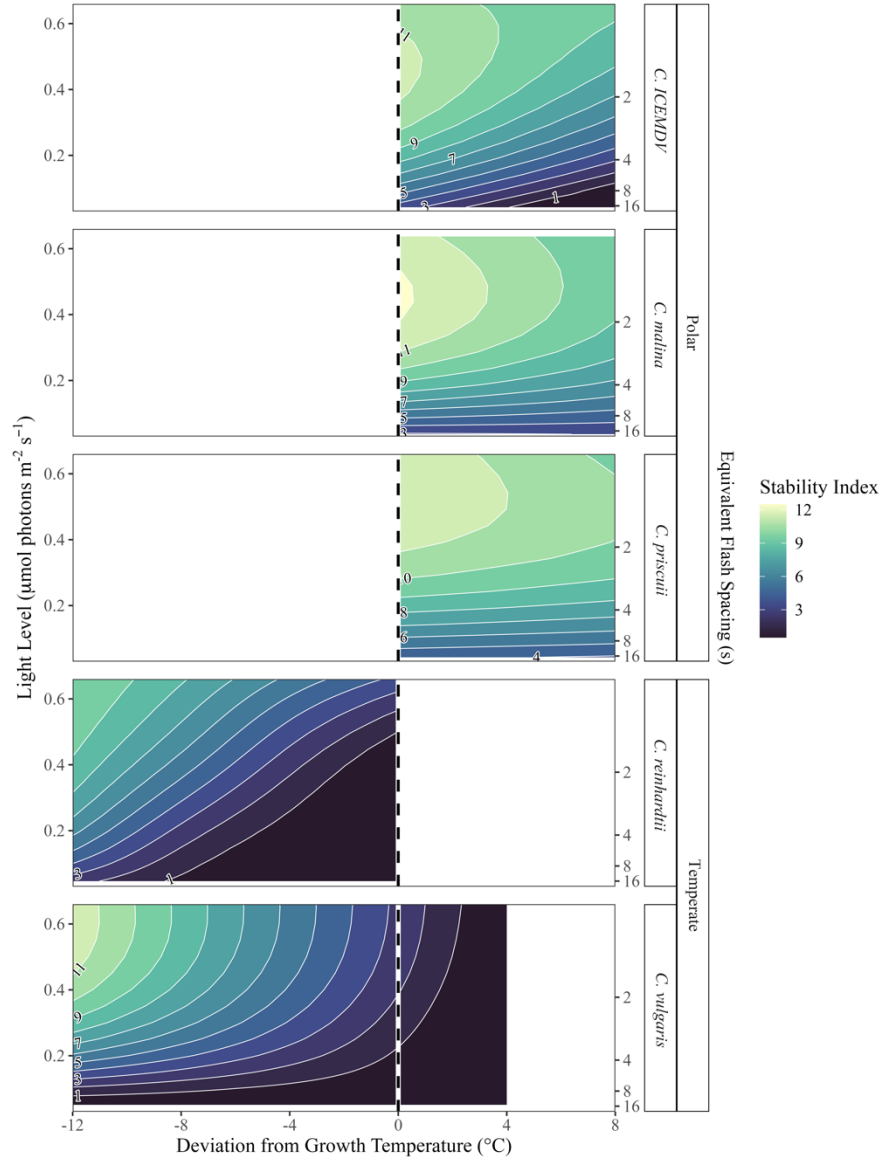


Figure 12: GAM model predictions of the consecutive flashes before the damping of S-State-induced chlorophyll fluorescence oscillations as predicted by the deviation from growth temperature ($^{\circ}\text{C}$) during measurements and the equivalent light level ($\mu\text{mol photons m}^{-2}\text{s}^{-1}$, with flash spacings in seconds) experienced by polar and temperate green algae. Dashed vertical lines represent the growth temperatures.

Generalized Additive Modelling By Measurement Temperature

To facilitate comparison across actual measurement temperatures, additional generalized additive models were fit to the data. For *T. pseudonana*, *C. ICEMDV*, *C. priscuii*, *C. malina*, *C. reinhardtii*, and *C. vulgaris*, replicate cultures of the strain were grown at the same temperatures. Therefore, the GAMs generated for these strains encompass a different temperature range but are represented by the same summary statistics (Table 4). Conversely, the polar diatom *F. cylindrus* was cultured at both 0 and 6°C. Thus, separate models were fit for each *F. cylindrus* culture to account for possible physiological differences resulting from the distinct growth conditions.

The smoothing term was significant for both *F. cylindrus* cultures (0°C $F = 4.46$, $p = 0.00827$; 6°C $F = 3.42$, $p = 0.0279$). However, while the model accounted for 73.4% of the deviance in the damping response of *F. cylindrus* grown at 0°C (adjusted $R^2 = 0.609$), it only accounted for 65.1% (adjusted $R^2 = 0.509$) in *F. cylindrus* grown at 6°C (Table 4).

Table 4: Summary statistics by phytoplankton strain of GAM models using the restricted maximum likelihood method to model the response of the damping of S-State-induced chlorophyll fluorescence oscillations to the predictors of measurement temperature (°C) and the equivalent light level ($\mu\text{mol photons m}^{-2}\text{s}^{-1}$).

Strain	Significance of smooth term			Adjusted R^2	Deviance Explained
	EDF	F-ratio	P-value		
<i>F. cylindrus</i> (grown at 0°C)	6.06	4.46	0.00827	0.609	73.4%
<i>F. cylindrus</i> (grown at 6°C)	5.49	3.42	0.0279	0.509	65.1%
<i>T. pseudonana</i>	6.08	9.01	5.38e-06	0.674	73.2%
<i>C. ICEMDV</i>	4.51	6.59	0.00687	0.687	78.8%
<i>C. priscuii</i>	4.31	2.17	0.115	0.389	57.7%
<i>C. malina</i>	4.34	2.56	0.0843	0.423	60.2%
<i>C. reinhardtii</i>	6.05	9.49	0.000274	0.786	85.4%
<i>C. vulgaris</i>	5.39	13.83	4.08e-06	0.772	82.3%

Although measured at the same range of temperatures, the two *F. cylindrus* cultures from different growth temperatures exhibited different trends in ChlF oscillations. Firstly, the culture grown at 0°C exhibited the significant 4-step oscillation in ChlF indicative of synchronized S-State cycling across only 75% of the measured conditions, compared to 95% of the measurement conditions for the culture grown at 6°C (Figure 13). Further, at comparable measurement

temperatures under wide flash spacing, equivalent to low light, the culture grown at 6°C maintained significant ChlF oscillations for longer (Figure 14). At flash spacings equivalent to light levels above 0.2 $\mu\text{mol photons m}^{-2}\text{s}^{-1}$, cultures from both 0 and 6°C growth temperatures exhibited similar, consistent stability indices (Figure 14).

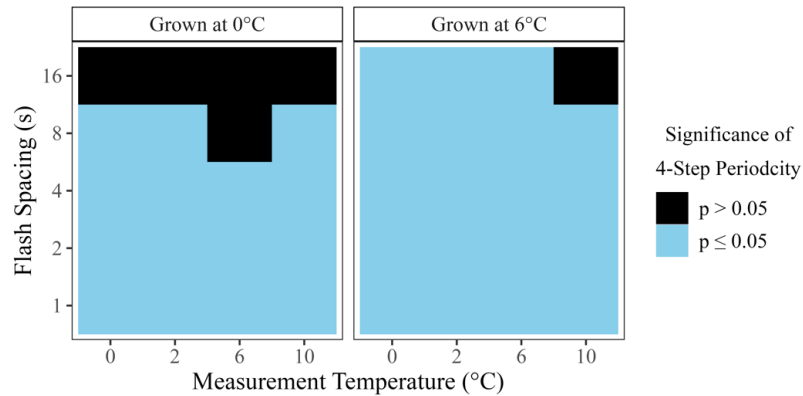


Figure 13: Statistical significance of 4-step oscillations in the maximum quantum yield of PSII photochemistry across measurement conditions in the polar diatom *F. cylindrus*, as measured through variable chlorophyll fluorescence.

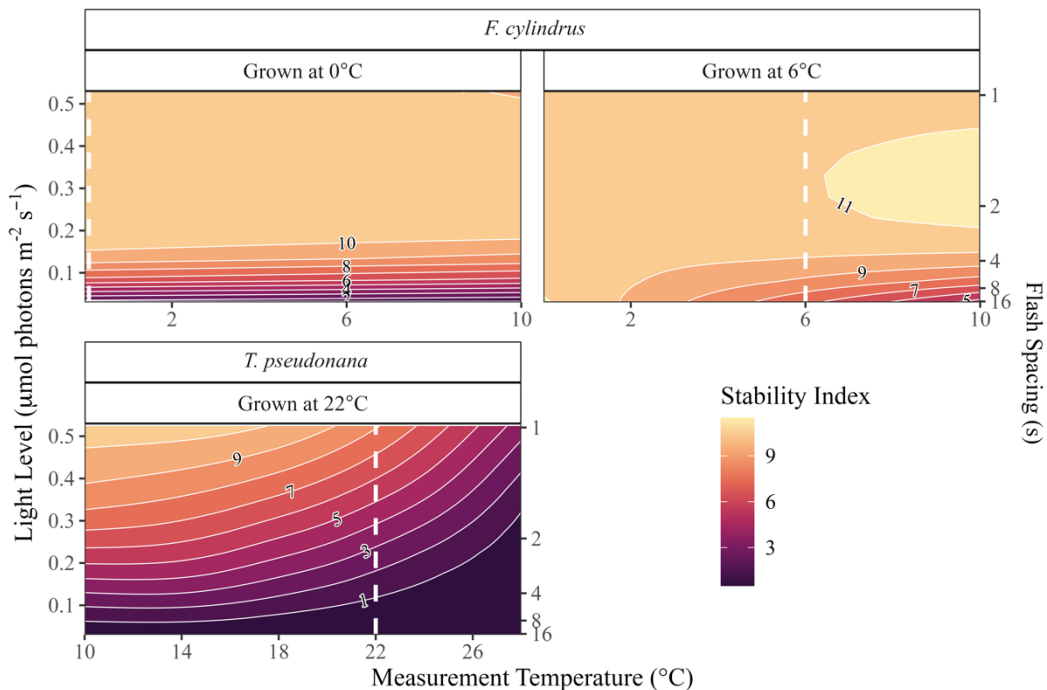


Figure 14: GAM model predictions of the consecutive flashes before the damping of S-State-induced chlorophyll fluorescence oscillations as predicted by the measurement temperature ($^{\circ}\text{C}$) and equivalent light level ($\mu\text{mol photons m}^{-2}\text{s}^{-1}$; with flash spacings in seconds) experienced by polar and temperate diatoms. White dashed vertical lines represent the growth temperatures of the individual cultures.

At a measurement temperature of 10°C, the model predicts that the duration of ChlF oscillations (stability index) for *F. cylindrus* will sharply increase with equivalent light before plateauing at approximately 0.2 $\mu\text{mol photons m}^{-2}\text{s}^{-1}$, produced by a 4-second interval between flashes (Figure 15). At light levels below 0.5 $\mu\text{mol photons m}^{-2}\text{s}^{-1}$, this corresponds to *F. cylindrus* exhibiting more sustained ChlF oscillations than does *T. pseudonana* also measured at 10°C. However, at this common measurement temperature and the higher equivalent light levels produced by shorter flash spacings, *T. pseudonana* sustains stable ChlF oscillations comparably to its polar counterpart *F. cylindrus* (Figure 15).

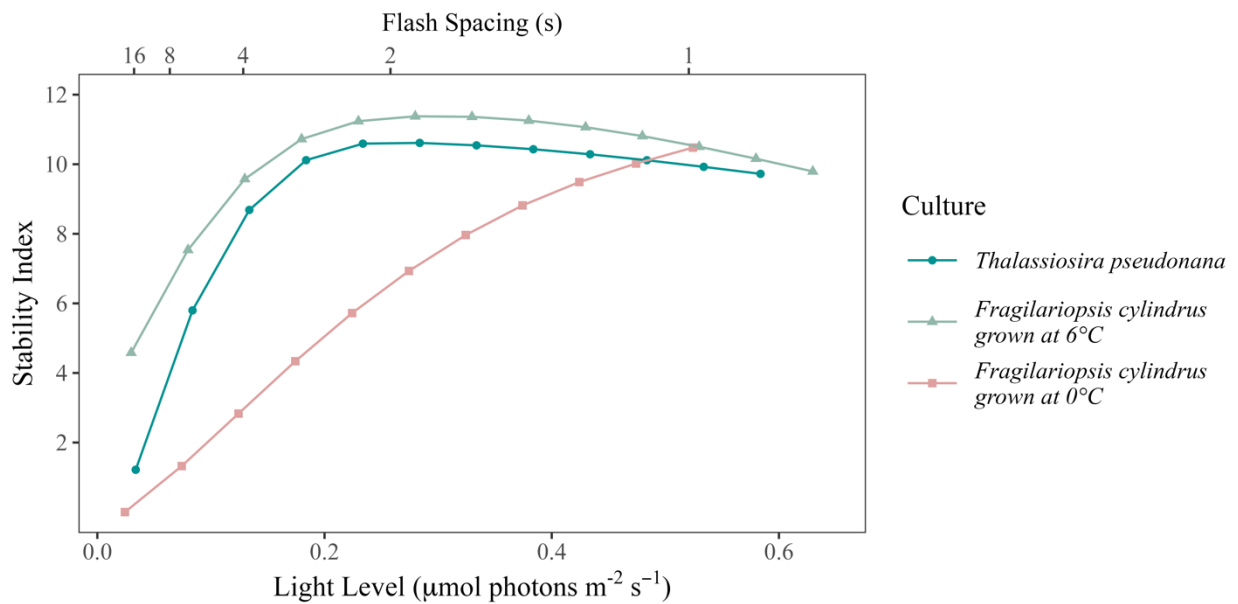


Figure 15: GAM model predictions of the consecutive flashes before the damping of S-State-induced chlorophyll fluorescence oscillations in polar and temperate diatom cultures over a range of equivalent light levels ($\mu\text{mol photons m}^{-2}\text{s}^{-1}$) at a common measurement temperature of 10°C. The equivalent light levels for the model training data were calculated based on the spacing (seconds) between sequential flashes delivered to the culture.

For the green algae, the models using measurement temperature as a predictor depicted similar trends between and within strains as the models using the deviation from growth temperature as a predictor (Figure 16).

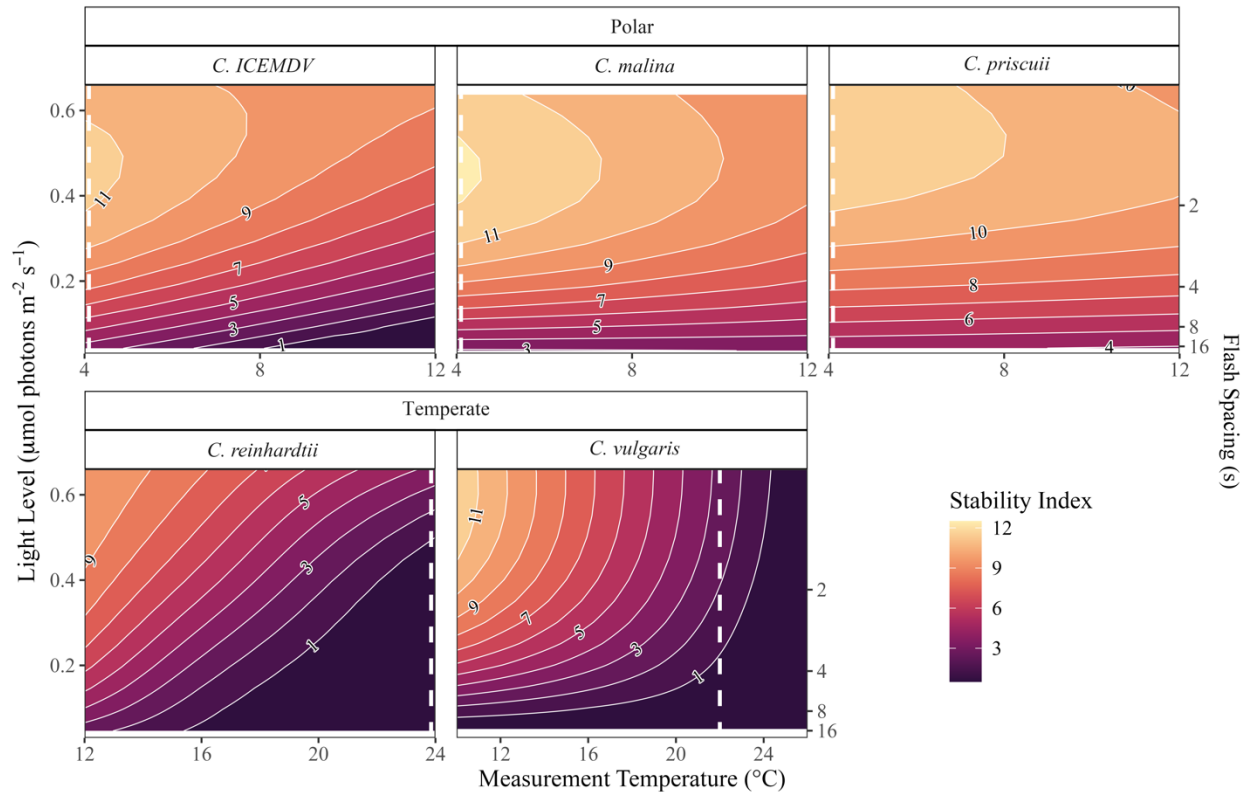


Figure 16: GAM model predictions of the consecutive flashes before the damping of S-State-induced chlorophyll fluorescence oscillations as predicted by the measurement temperature ($^{\circ}\text{C}$) and the equivalent light level ($\mu\text{mol photons m}^{-2}\text{s}^{-1}$; with flash spacings in seconds) experienced by polar and temperate green algae. White dashed lines represent the growth temperatures of the individual strains.

However, the model predictions at a shared measurement temperature of 12°C demonstrate limited variation among green algal taxa (Figure 17). For all green algal strains, the duration of significant ChlF oscillations increased with the higher equivalent light levels corresponding to shorter intervals between sequential flashes. Two polar strains, *C. priscui* and *C. malina*, and the temperate *C. reinhardtii* showed near-identical trajectories. While the temperate *C. vulgaris* exhibits less sustained ChlF oscillations at low equivalent light levels, it achieves similar stability to the *Chlamydomonas* strains by flash spacings of 2 seconds, equivalent to an equivalent light level of approximately $0.3 \mu\text{mol photons m}^{-2}\text{s}^{-1}$. Unexpectedly, the polar alga *C. ICEMDV* consistently exhibits the shortest stability of ChlF oscillations, indicative of the least sustained S-State cycling across all measurement conditions (Figure 17).

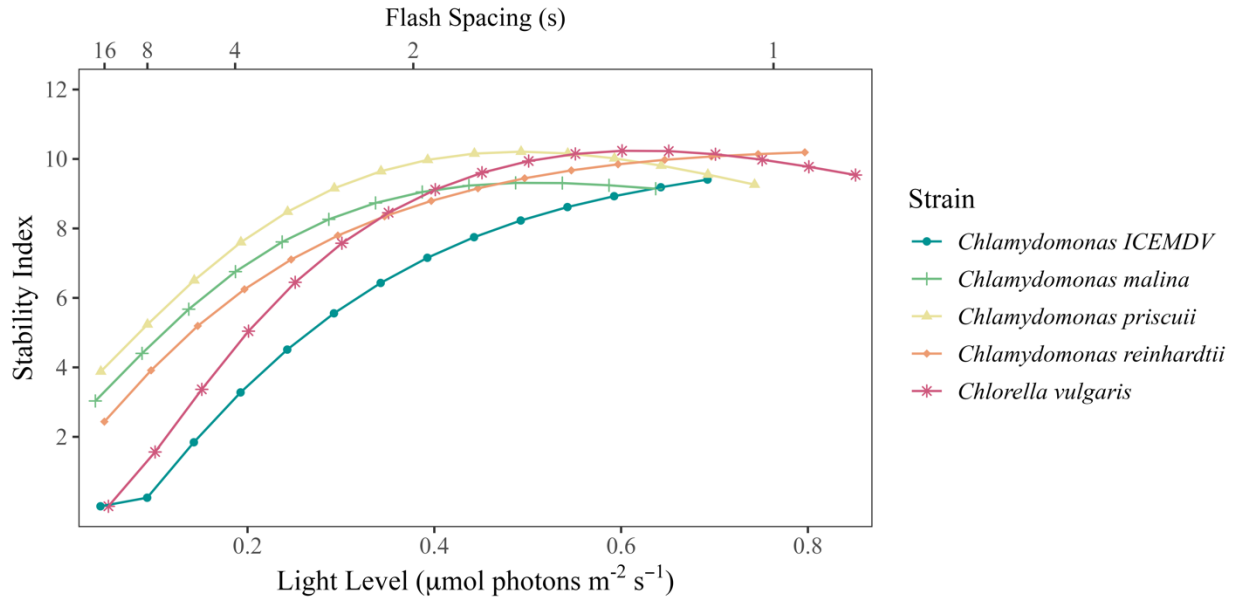


Figure 17: GAM model predictions of the consecutive flashes before the damping of S-State-induced chlorophyll fluorescence oscillations in polar and temperate green algae strains over a range of equivalent light levels ($\mu\text{mol photons m}^{-2}\text{s}^{-1}$) at a common measurement temperature of 12°C . The equivalent light levels for the model training data were calculated based on the spacing (seconds) between sequential flashes delivered to the culture.

Discussion

Modelling and Operational Limitations

Two generalized additive models were fit for each phytoplankton strain, predicting the number of consecutive flashes before the damping of ChlF oscillations based on the equivalent light level ($\mu\text{mol photons m}^{-2}\text{s}^{-1}$), and either the measurement temperature or the deviation from the growth temperature during measurement ($^{\circ}\text{C}$; Tables 3 & 4). All models explained over 50% of the deviance in the response variable. Additionally, the tensor product smooth of the predictors was statistically significant in both models for *F. cylindrus*, *T. pseudonana*, *C. ICEMDV*, *C. reinhardtii*, and *C. vulgaris*. However, for two strains of polar green algae, *C. priscuii* and *C. malina*, the tensor product smooths of the predictors were not statistically significant.

The insignificance of the tensor product smooth for *C. malina* can be attributed to a significant outlier in the model training data (see model training dataset at [GitHub: S-State Damping](#)). Evaluating the Cook's distances [65], an outlier occurs at a measurement temperature of 12°C and a 2-second interval between flashes (corresponding to an equivalent light level of $0.073 \mu\text{mol photons m}^{-2}\text{s}^{-1}$). Under these conditions, significant ChlF oscillations were detected over nine flashes, a sharp contrast to the closest other conditions, which exhibited no significant 4-step oscillations in ChlF (stability index of 0). Removing this outlier point increases the deviation explained by the model from 60.2 to 75.2 % and produces a significant smooth term ($F = 4.544$, $p = 0.0255$).

Conversely, the insignificance of the smooth term in *C. priscuii* is attributable to the limited number of measurement temperatures. With only three measurement temperatures, the number of basis dimensions used to create the smooth function (k) was limited to 3 [63]. However, model validation demonstrates that three basis dimensions cannot capture the underlying relationship between the predictors and the response variable (Table A2). Therefore, three measurement temperatures were insufficient for modelling the response of ChlF damping for this strain.

Beyond the modelling limitations, ignoring the limited range of equivalent light levels evaluated in this study would be remiss. Our overall measurement range of 0.024 to $0.898 \mu\text{mol photons m}^{-2}\text{s}^{-1}$ (Table 2) is approximately three to five orders of magnitude lower than full

sunlight and approximately one to three orders of magnitude below the traditional threshold for the bottom of the photic zone in the ocean [2].

The operational capacity of the Soliense LIFT-REM fluorometer bounded the upper limit of the measurable equivalent light range. In an analysis comprising 425 runs, the set flash spacing was compared to the actual spacing recorded between flashes down to the millisecond. In runs with the flash spacing set to 0.5, 0.25, or 0.1 seconds, the average measured flash spacings were 1.06, 1.00, and 1.00, respectively (see Appendix Table 1). Thus, a 1-second interval was the lowest reliable flash spacing, corresponding to maximum equivalent light levels of 0.534 to 0.898 $\mu\text{mol photons m}^{-2}\text{s}^{-1}$, depending on the equivalent absorption cross-section of photosystem II (σ_{PSII}) of each culture (Table 2).

Consistent Responses to Measurement Conditions

Across all study strains, the observed ChlF oscillations indicate less efficient photosynthetic energy conversion under higher temperatures and lower light levels. The wavelet power at a period of four declines with decreasing light and with increasing temperatures, illustrating that the periodic oscillations in ChlF are weaker under these conditions (Figure 9). Further, the decrease in the consecutive flashes before the ChlF oscillations damp out suggests that cultures are maintaining synchronicity in their S-State cycling for shorter durations (Figure 14, 16) [31]. The desynchronization of S-State cycling between the PSII in a population indicates that a sufficient number of charge recombinations have taken place to create a PSII population with a randomized distribution of S-States. Thus, if this desynchronization occurs after fewer consecutive flashes, it signifies an increased proportion of PSII undergoing charge recombinations after each flash. By inference, PSII populations with increased incidence of energetically wasteful charge recombinations, such as those under high temperatures and low light levels, are less efficient in their photosynthetic energy conversion [23].

These results are consistent with previous literature evaluating the response of recombination reactions to light conditions. As light levels decline, there are longer intervals between successive PSII excitations, pushing fewer electrons through the electron transport chain [30]. Consequently, the probability of energetically wasteful charge recombinations is higher, corresponding to weaker maintenance of S-State cycling [30,31]. Similarly, these findings are consistent with known relationships between charge recombination and temperature, as

recombination reactions typically decrease with temperature due to the thermal sensitivity of the associated enzymes [50]. However, these results are in direct contrast with previous literature regarding the temperature dependence of S-State transitions. In 2022, Han *et al.* compared the miss probability of S-State transitions at -10, 1, 10, and 20 °C. Applying a variable series of flashes to isolated PSII in temperature-controlled ethanol baths, they demonstrated that the average miss probability of S-State transitions was highest at -10 °C and lowest at 10 °C [66]. Therefore, we would expect to have seen more sustained S-State transitions at moderate temperatures.

Comparisons Among Strains

Polar strains of diatoms and green algae consistently demonstrated a stronger periodicity in ChlF emissions (Figure 9). Further, they exhibited significant 4-step ChlF oscillations under a broader range of measurement conditions (Figure 10) than did their temperate counterparts. These findings illustrate that polar phytoplankton strains have a higher capacity to maintain S-State cycling than do temperate strains. Nevertheless, comparing the number of consecutive flashes before the ChlF oscillations damp out between strains under comparable conditions reveals variable patterns.

The first comparison was between the polar diatom *F. cylindrus* and the temperate diatom *T. pseudonana*. When measured at the same temperature under low light, *F. cylindrus* sustained ChlF oscillations for longer than *T. pseudonana*. However, as light levels increased, the stability of cycling in *T. pseudonana* increased to near that of *F. cylindrus* (Figure 15). This behaviour is consistent with the trends observed below the growth temperature when comparing these two diatom strains by the deviation from growth temperature during measurement (Figure 11). Yet, when temperatures increase the same amount above the growth temperature, *F. cylindrus* maintains cycling for much longer than *T. pseudonana*, regardless of the light level. These trends indicate that *F. cylindrus* maintains S-State cycling for longer than *T. pseudonana* under low photon delivery and low temperatures. However, in less stressful conditions, *T. pseudonana* can match the photosynthetic performance of *F. cylindrus*. Theoretically, the rate of charge recombinations should increase under low light and higher temperatures [30,50]. Thus, the stability of S-State cycling in the PSII of *F. cylindrus* under these conditions supports a

suppression of energetically wasteful charge recombinations by the polar strain compared to a temperate diatom.

The second comparison comprises three polar, *C. priscuii*, *C. malina*, and *C. ICEMDV*, and two temperate, *C. reinhardtii*, and *C. vulgaris*, strains of green algae. When evaluated at their growth temperature, the polar strains maintained significant ChlF oscillations for more flash cycles, than did their temperate counterparts across all light conditions (Figure 12). Yet, when compared at the same measurement temperature, these strains showed little variation in the stability of significant ChlF oscillations (Figure 17), suggesting little difference in the incidence of energetically wasteful charge recombinations. This shared measurement temperature represents a departure from the growth temperature of +8 °C for polar strains and -10 to -12 °C for temperate strains. Recombination reactions are expected to increase with temperature [50]. Thus, the capacity for polar strains to exhibit the same stability of S-State cycling when warmed, as temperate strains do when cooled, suggests some suppression of energetically wasteful charge recombinations in the PSII of polar strains. This finding is underscored by the disparity in recombination reactions observed when measured under the same offset from growth temperature and equivalent light.

Through analyzing ChlF oscillations, we extrapolated the stability of significant S-State cycling and therefore, the incidence of energetically wasteful charge recombinations. Overall, our findings indicate that polar phytoplankton exhibit more stable S-State cycling than do temperate strains under limited light and temperatures surpassing their growth conditions. These findings suggest that polar phytoplankton strains increase their photosynthetic energy conversion efficiency under low light and low temperatures by minimizing energetically wasteful charge recombinations. Stable S-State cycling and minimal energy loss through charge recombination ensure continued electron flow through the ETC, sustaining ATP and NADPH production, and minimizing the risk of photodamage to the photosynthetic machinery [23,30]. Thus, stable S-State cycling, with inferred suppression of wasteful recombinations, may be integral for the productivity of polar phytoplankton under the ice during the polar night.

Ecological Implications & Future Directions

Unravelling the mechanisms enabling polar phytoplankton to sustain slow, but significant productivity under the ice in the winter is crucial for predicting the changing dynamics of spring phytoplankton blooms. This is particularly critical in the Arctic, where the pace of warming is rapidly accelerating [7]. Beyond temperature changes, polar aquatic ecosystems are experiencing reductions in sea ice extent and thickness, escalating freshwater inputs, acidification, and increased winds and storms [7,12]. These pressures are causing alterations in the productivity and seasonal peaks of phytoplankton blooms [7,11]. Understanding the nature of maintaining an intact photosystem under the ice in the winter allows us to better predict under what conditions these blooms will initiate, and which phytoplankton strains will be involved [4].

The ability to maintain efficient photosynthetic energy conversion over winter is crucial for the timing and speed of spring bloom initiation [4]. Strains with this ability may possess a competitive advantage in quickly initiating spring growth, giving them first access to the nutrients required to form an extensive bloom. Thus, the proportions of these strains may increase in polar regions. Altering the phytoplankton community composition may, in turn, exert bottom-up effects on polar ecosystems [7].

Future directions for this research include more extensive comparative analyses to further our understanding. Incorporating more strains of diatoms and green algae, as well as other phytoplankton groups will enable us to uncover whether certain groups have a higher capacity to suppress energetically wasteful charge recombinations. A difference between these groups may affect their contribution to the phytoplankton community, leading to differences in the ecosystem services offered by spring phytoplankton blooms. Moreover, since there were differences observed between *F. cylindrus* strains grown at 0 and 6 °C, further comparison between ecotypes may yield information on the conditions that lead to the evolution of this ability.

References

1. Pierella Karlusich JJ, Ibarbalz FM, Bowler C. Phytoplankton in the Tara Ocean. *Annual Review of Marine Science*. 2020;12: 233–265. doi:10.1146/annurev-marine-010419-010706
2. Raven JA, Kübler JE, Beardall J. Put out the light, and then put out the light. *Journal of the Marine Biological Association of the United Kingdom*. 2000;80: 1–25. doi:10.1017/S0025315499001526
3. Kirk JTO. *Light and Photosynthesis in Aquatic Ecosystems*. 3rd ed. Cambridge, UK: Cambridge University Press; 2011.
4. Randelhoff A, Lacour L, Marec C, Leymarie E, Lagunas J, Xing X, et al. Arctic mid-winter phytoplankton growth revealed by autonomous profilers. *Science Advances*. 2020;6: eabc2678. doi:10.1126/sciadv.abc2678
5. Hancke K, Lund-Hansen LC, Lamare ML, Højlund Pedersen S, King MD, Andersen P, et al. Extreme Low Light Requirement for Algae Growth Underneath Sea Ice: A Case Study From Station Nord, NE Greenland. *Journal of Geophysical Research: Oceans*. 2018;123: 985–1000. doi:10.1002/2017JC013263
6. Leu E, Mundy CJ, Assmy P, Campbell K, Gabrielsen TM, Gosselin M, et al. Arctic spring awakening – Steering principles behind the phenology of vernal ice algal blooms. *Progress in Oceanography*. 2015;139: 151–170. doi:10.1016/j.pcean.2015.07.012
7. Ardyna M, Arrigo KR. Phytoplankton dynamics in a changing Arctic Ocean. *Nat Clim Chang*. 2020;10: 892–903. doi:10.1038/s41558-020-0905-y
8. Robinson DH, Arrigo KR, Iturriaga R, Sullivan CW. Microalgal Light-Harvesting in Extreme Low-Light Environments in Mcmurdo Sound, Antarctica. *Journal of Phycology*. 1995;31: 508–520. doi:10.1111/j.1529-8817.1995.tb02544.x
9. Bax N, Sands CJ, Gogarty B, Downey RV, Moreau CVE, Moreno B, et al. Perspective: Increasing blue carbon around Antarctica is an ecosystem service of considerable societal and economic value worth protecting. *Glob Chang Biol*. 2021;27: 5–12. doi:10.1111/gcb.15392
10. Lyon BR, Mock T. Polar Microalgae: New Approaches towards Understanding Adaptations to an Extreme and Changing Environment. *Biology*. 2014;3: 56–80. doi:10.3390/biology3010056
11. Croteau D, Guérin S, Bruyant F, Ferland J, Campbell DA, Babin M, et al. Contrasting nonphotochemical quenching patterns under high light and darkness aligns with light niche occupancy in Arctic diatoms. *Limnology and Oceanography*. 2021;66: S231–S245. doi:10.1002/lno.11587

12. Cvetkovska M, Vakulenko G, Smith DR, Zhang X, Hüner NPA. Temperature stress in psychrophilic green microalgae: Minireview. *Physiologia Plantarum*. 2022;174: e13811. doi:10.1111/ppl.13811
13. Mock T, Otilar RP, Strauss J, McMullan M, Paajanen P, Schmutz J, et al. Evolutionary genomics of the cold-adapted diatom *Fragilariopsis cylindrus*. *Nature*. 2017;541: 536–540. doi:10.1038/nature20803
14. Bayer-Giraldi M, Weikusat I, Besir H, Dieckmann G. Characterization of an antifreeze protein from the polar diatom *Fragilariopsis cylindrus* and its relevance in sea ice. *Cryobiology*. 2011;63: 210–219. doi:10.1016/j.cryobiol.2011.08.006
15. Kennedy F, Martin A, Bowman JP, Wilson R, McMinn A. Dark metabolism: a molecular insight into how the Antarctic sea-ice diatom *Fragilariopsis cylindrus* survives long-term darkness. *New Phytologist*. 2019;223: 675–691. doi:10.1111/nph.15843
16. Luciński R, Jackowski G. The structure, functions and degradation of pigment-binding proteins of photosystem II. *Acta Biochimica Polonica*. 2006;53: 693–708. doi:10.18388/abp.2006_3297
17. Kawakami K, Shen J-R. Purification of fully active and crystallizable photosystem II from thermophilic cyanobacteria. *Methods in Enzymology*. Elsevier; 2018. pp. 1–16. doi:10.1016/bs.mie.2018.10.002
18. Vass I. Role of charge recombination processes in photodamage and photoprotection of the photosystem II complex. *Physiologia Plantarum*. 2011;142: 6–16. doi:10.1111/j.1399-3054.2011.01454.x
19. Schuback N, Tortell PD, Berman-Frank I, Campbell DA, Ciotti A, Courtecuisse E, et al. Single-Turnover Variable Chlorophyll Fluorescence as a Tool for Assessing Phytoplankton Photosynthesis and Primary Productivity: Opportunities, Caveats and Recommendations. *Frontiers in Marine Science*. 2021;8. doi:10.3389/fmars.2021.690607
20. Shen J-R. Photosynthesis | Photosystem II: Protein Components, Structure and Electron Transfer. In: Jez J, editor. *Encyclopedia of Biological Chemistry III (Third Edition)*. Oxford: Elsevier; 2021. pp. 215–228. doi:10.1016/B978-0-12-819460-7.00012-8
21. Mukhopadhyay S, Mandal SK, Bhaduri S, Armstrong WH. Manganese Clusters with Relevance to Photosystem II. *Chem Rev*. 2004;104: 3981–4026. doi:10.1021/cr0206014
22. Vass I, Cser K. Janus-faced charge recombinations in photosystem II photoinhibition. *Trends in Plant Science*. 2009;14: 200–205. doi:10.1016/j.tplants.2009.01.009
23. Rappaport F, Cuni A, Xiong L, Sayre R, Lavergne J. Charge Recombination and Thermoluminescence in Photosystem II. *Biophysical Journal*. 2005;88: 1948–1958. doi:10.1529/biophysj.104.050237

24. Laloi C, Przybyla D, Apel K. A genetic approach towards elucidating the biological activity of different reactive oxygen species in *Arabidopsis thaliana*. *Journal of Experimental Botany*. 2006;57: 1719–1724. doi:10.1093/jxb/erj183
25. Rutherford AW, Osyczka A, Rappaport F. Back-reactions, short-circuits, leaks and other energy wasteful reactions in biological electron transfer: Redox tuning to survive life in O₂. *FEBS Letters*. 2012;586: 603–616. doi:10.1016/j.febslet.2011.12.039
26. Vinyard DJ, Ananyev GM, Charles Dismukes G. Photosystem II: The Reaction Center of Oxygenic Photosynthesis. *Annual Review of Biochemistry*. 2013;82: 577–606. doi:10.1146/annurev-biochem-070511-100425
27. Gates C, Ananyev G, Dismukes GC. Realtime kinetics of the light driven steps of photosynthetic water oxidation in living organisms by “stroboscopic” fluorometry. *Biochimica et Biophysica Acta (BBA) - Bioenergetics*. 2020;1861: 148212. doi:10.1016/j.bbabi.2020.148212
28. Zaharieva I, Dau H. Energetics and Kinetics of S-State Transitions Monitored by Delayed Chlorophyll Fluorescence. *Frontiers in Plant Science*. 2019;10. Available: <https://www.frontiersin.org/articles/10.3389/fpls.2019.00386>
29. Dau H, Haumann M. Time-resolved X-ray spectroscopy leads to an extension of the classical S-state cycle model of photosynthetic oxygen evolution. *Photosynth Res*. 2007;92: 327–343. doi:10.1007/s11120-007-9141-9
30. Keren N, Berg A, van Kan PJM, Levanon H, Ohad I. Mechanism of photosystem II photoinactivation and D1 protein degradation at low light: The role of back electron flow. *Proceedings of the National Academy of Sciences*. 1997;94: 1579–1584. doi:10.1073/pnas.94.4.1579
31. de Wijn R, van Gorkom HJ. S-state dependence of the miss probability in Photosystem II. *Photosynthesis Research*. 2002;72: 217–222. doi:10.1023/A:1016128632704
32. Otte A, Winder JC, Deng L, Schmutz J, Jenkins J, Grigoriev IV, et al. The diatom *Fragilariopsis cylindrus*: A model alga to understand cold-adapted life. *Journal of Phycology*. 2023;59: 301–306. doi:10.1111/jpy.13325
33. Cefarelli AO, Ferrario ME, Almandoz GO, Atencio AG, Akselman R, Vernet M. Diversity of the diatom genus *Fragilariopsis* in the Argentine Sea and Antarctic waters: morphology, distribution and abundance. *Polar Biology*. 2010;33. doi:10.1007/s00300-010-0794-z
34. Kang S-H, Fryxell GA. *Fragilariopsis cylindrus* (Grunow) Krieger: The most abundant diatom in water column assemblages of Antarctic marginal ice-edge zones. *Polar Biol*. 1992;12: 609–627. doi:10.1007/BF00236984
35. Poulsen N, Kröger N. *Thalassiosira pseudonana* (*Cyclotella nana*) (Hustedt) Hasle et Heimdal (Bacillariophyceae): A genetically tractable model organism for studying diatom

- biology, including biological silica formation. *Journal of Phycology*. 2023;59: 809–817. doi:10.1111/jpy.13362
36. Cook G, Teufel A, Kalra I, Li W, Wang X, Priscu J, et al. The Antarctic psychrophiles *Chlamydomonas* spp. *UWO241* and *ICEMDV* exhibit differential restructuring of photosystem I in response to iron. *Photosynth Res*. 2019;141: 209–228. doi:10.1007/s11120-019-00621-0
 37. Stahl-Rommel S, Kalra I, D’Silva S, Hahn MM, Popson D, Cvetkovska M, et al. Cyclic electron flow (CEF) and ascorbate pathway activity provide constitutive photoprotection for the photopsychrophile, *Chlamydomonas* sp. *UWO 241* (renamed *Chlamydomonas priscuii*). *Photosynth Res*. 2022;151: 235–250. doi:10.1007/s11120-021-00877-5
 38. Li W, Podar M, Morgan-Kiss RM. Ultrastructural and Single-Cell-Level Characterization Reveals Metabolic Versatility in a Microbial Eukaryote Community from an Ice-Covered Antarctic Lake. *Applied and Environmental Microbiology*. 2016;82: 3659–3670. doi:10.1128/AEM.00478-16
 39. Hüner NPA, Szyszka-Mroz B, Ivanov AG, Kata V, Lye H, Smith DR. Photosynthetic adaptation and multicellularity in the Antarctic psychrophile, *Chlamydomonas priscuii*. *Algal Research*. 2023;74: 103220. doi:10.1016/j.algal.2023.103220
 40. Balzano S, Gourvil P, Siano R, Chanoine M, Marie D, Lessard S, et al. Diversity of cultured photosynthetic flagellates in the northeast Pacific and Arctic Oceans in summer. *Biogeosciences*. 2012;9: 4553–4571. doi:10.5194/bg-9-4553-2012
 41. Morales-Sánchez D, Schulze PSC, Kiron V, Wijffels RH. Temperature-Dependent Lipid Accumulation in the Polar Marine Microalga *Chlamydomonas malina* RCC2488. *Frontiers in Plant Science*. 2020;11. doi:10.3389/fpls.2020.619064
 42. Sasso S, Stibor H, Mittag M, Grossman AR. From molecular manipulation of domesticated *Chlamydomonas reinhardtii* to survival in nature. King SR, Rodgers PA, editors. *eLife*. 2018;7: e39233. doi:10.7554/eLife.39233
 43. Xie B, Bishop S, Stessman D, Wright D, Spalding MH, Halverson LJ. *Chlamydomonas reinhardtii* thermal tolerance enhancement mediated by a mutualistic interaction with vitamin B12-producing bacteria. *The ISME Journal*. 2013;7: 1544–1555. doi:10.1038/ismej.2013.43
 44. Wiel JBV, D. Mikulicz J, R. Boysen M, Hashemi N, Kalgren P, M. Nauman L, et al. Characterization of *Chlorella vulgaris* and *Chlorella protothecoides* using multi-pixel photon counters in a 3D focusing optofluidic system. *RSC Advances*. 2017;7: 4402–4408. doi:10.1039/C6RA25837A
 45. Leyva LA, Bashan Y, Mendoza A, de-Bashan LE. Accumulation fatty acids of in *Chlorella vulgaris* under heterotrophic conditions in relation to activity of acetyl-CoA carboxylase, temperature, and co-immobilization with *Azospirillum brasilense*. *Naturwissenschaften*. 2014;101: 819–830. doi:10.1007/s00114-014-1223-x

46. Suggest DJ, Moore CM, Oxborough K, Geider RJ. Fast Repetition Rate (FRR) Chlorophyll a Fluorescence Induction Measurements. University of Essex; 2006.
47. Berman-Frank I, Campbell D, Ciotti A, Erickson Z, Fujiki T, Halsey K, et al. Application of Single Turnover Active Chlorophyll Fluorescence for Phytoplankton Productivity Measurements. Version 2.0. Scientific Committee on Oceanic Research (SCOR) Working Group 156; 2023 Jun. doi:10.25607/OBP-1084
48. Kolber ZS. Measurements of variable chlorophyll fluorescence using fast repetition rate techniques: defining methodology and experimental protocols. *Biochimica et Biophysica Acta*. 1998;1367: 19. doi:10.1016/S0005-2728(98)00135-2
49. Xu K, Lavaud J, Perkins R, Austen E, Bonnanfant M, Campbell DA. Phytoplankton σ PSII and Excitation Dissipation; Implications for Estimates of Primary Productivity. *Front Mar Sci*. 2018;5. doi:10.3389/fmars.2018.00281
50. Ivanov AG, Sane PV, Krol M, Gray GR, Balseris A, Savitch LV, et al. Acclimation to temperature and irradiance modulates PSII charge recombination. *FEBS Letters*. 2006;580: 2797–2802. doi:10.1016/j.febslet.2006.04.018
51. Wickham H, Averick M, Bryan J, Chang W, McGowan LD, François R, et al. Welcome to the tidyverse. *Journal of Open Source Software*. 2019;4: 1686. doi:10.21105/joss.01686
52. Grolemund G, Wickham H. Dates and times made easy with lubridate. *Journal of Statistical Software*. 2011;40: 1–25. doi:10.18637/jss.v040.i03
53. Bryan J. googlesheets4: Access google sheets using the sheets API V4. 2023. Available: <https://github.com/tidyverse/googlesheets4>
54. Højsgaard S, Halekoh U. doBy: Groupwise statistics, LSmeans, linear estimates, utilities. 2023. Available: <https://CRAN.R-project.org/package=doBy>
55. Roesch A, Schmidbauer H. WaveletComp: Computational wavelet analysis. 2018. Available: <https://CRAN.R-project.org/package=WaveletComp>
56. Wood SN. Fast stable restricted maximum likelihood and marginal likelihood estimation of semiparametric generalized linear models. *Journal of the Royal Statistical Society: Series B (Statistical Methodology)*. 2011;73: 3–36. doi:10.1111/j.1467-9868.2010.00749.x
57. Fasiolo, Matteo, Nedellec, Rapha"el, Goude, Yannig, et al. Scalable visualisation methods for modern generalized additive models. *Journal of the Royal Statistical Society (B)*. 2020;29: 78–86. doi:10.1080/10618600.2019.1629942
58. Wickham H. ggplot2: Elegant graphics for data analysis. Springer-Verlag New York; 2016. Available: <https://ggplot2.tidyverse.org>
59. Campitelli E. metR: Tools for easier analysis of meteorological fields. 2021. doi:10.5281/zenodo.2593516

60. Theis FJ, Meyer-Bäse A. Spectral Transformations. 1st ed. Biomedical Signal Analysis : Contemporary Methods and Applications. 1st ed. MIT Press; 2010. p. 42.
61. Cazelles B, Chavez M, Berteaux D, Ménard F, Vik JO, Jenouvrier S, et al. Wavelet analysis of ecological time series. *Oecologia*. 2008;156: 287–304. doi:10.1007/s00442-008-0993-2
62. Pinilla J, Negrín M. Non-Parametric Generalized Additive Models as a Tool for Evaluating Policy Interventions. *Mathematics*. 2021;9: 299. doi:10.3390/math9040299
63. Schoenig D, Maynard L, Brice M-H, Cazelles K, Braga PHP, Gongora E, et al. Workshop 8: Generalized additive models in R. Québec Centre for Biodiversity Science; 2023. Available: <https://r.qcbs.ca/workshop08/pres-en/workshop08-pres-en.html#36>
64. Wood SN. Generalized Additive Models: an introduction with R. 2nd ed. New York: Chapman and Hall/CRC; 2017.
65. Yager RM. Detecting influential observations in nonlinear regression modeling of groundwater flow. *Water Resources Research*. 1998;34: 1623–1633. doi:10.1029/98WR01010
66. Han G, Chernev P, Styring S, Messinger J, Mamedov F. Molecular basis for turnover inefficiencies (misses) during water oxidation in photosystem II. *Chem Sci*. 2022;13: 8667–8678. doi:10.1039/D2SC00854H

Appendix

Table A1: Flash delivery capacity of the Soliense LIFT-REM fluorometer

Set Flash Spacing (s)	Mean Actual Flash Spacing (s)	Variance of Actual Flash Spacing (s)
0.1	1.00	3.86e-06
0.25	1.00	3.26e-06
0.5	1.06	8.84e-03
1	1.53	2.79e-03
2	2.54	2.74e-03
4	4.53	2.68e-03
8	8.54	2.90e-03
16	16.53	1.86e-03

Table A2: Basis dimension (k) checking results by phytoplankton strain of GAM models of the response of the damping of S-State-induced chlorophyll fluorescence oscillations to the predictors of measurement temperature (°C) and the equivalent light level ($\mu\text{mol photons m}^{-2}\text{s}^{-1}$). A low p-value (<0.05) indicates that K is too low.

Strain	K'	EDF	K-Index	P-Value
<i>C. ICEMDV</i>	8.00	4.51	1.27	0.91
<i>C. malina</i>	8.00	4.34	1.07	0.46
<i>C. priscuii</i>	8.00	4.31	0.67	0.02
<i>C. vulgaris</i>	24.00	5.39	1.29	0.99
<i>C. reinhardtii</i>	15.00	6.05	1.21	0.82
<i>T. pseudonana</i>	48.00	6.08	1.23	0.94
<i>F. cylindrus</i> (grown at 0 °C)	15.00	6.06	0.87	0.12
<i>F. cylindrus</i> (grown at 6 °C)	15.00	5.49	1.1	0.65